processes

MDPI

Article

Adaptive Non-Singular Terminal Sliding Mode Trajectory Tracking Control of Robotic Manipulators Based on Disturbance Observer Under Unknown Time-Varying Disturbance

Song Yin [1], Zhenjie Shi [1], Yanjun Liu [1,2,*], Gang Xue [1,2,3,*] and Huaqiang You [1]

[1] Key Laboratory of High-Efficiency and Clean Mechanical Manufacture of Ministry of Education, National Demonstration Center for Experimental Mechanical Engineering Education, School of Mechanical Engineering, Shandong University, Jinan 250061, China; yinsong1130@163.com (S.Y.); shizhenjie@mail.sdu.edu.cn (Z.S.); huaqiang_you@163.com (H.Y.)
[2] Institute of Marine Science and Technology, Shandong University, Qingdao 266237, China
[3] State Key Laboratory of Mechanical Transmission for Advanced Equipment, Chongqing University, Chongqing 400044, China
* Correspondence: lyj111yjslw@163.com (Y.L.); xuegangzb@163.com (G.X.)

Abstract: We address the problems in the trajectory tracking control of a multi-joint robotic arm, including uncertainty in the internal modeling of its significant external unknown time-varying disturbances. With the control objective of tracking the desired trajectories of each joint stably and accurately, this paper proposes an adaptive non-singular terminal sliding mode control method based on a nonlinear disturbance observer (NDO). In order to speed up the convergence of the tracking error and avoid the singular value problem existing in the traditional terminal sliding mode (TSM), a non-singular terminal sliding mode (NTSM) surface is proposed in this paper. Given the system modeling uncertainty and external unknown time-varying disturbances, a nonlinear disturbance observer is used to observe the total set disturbance for feed-forward compensation. Secondly, the switching gain adaptive law is used to estimate the observation error of the total set disturbance and allow for the online adjustment of the switching gain weights. A robust gain adaptive law is also designed to reconverge quickly to the non-singular sliding mode surface when transient significant disturbances shock the system's state variables out of the sliding phase. A simulation analysis of the spatial two-link robotic arm is carried out in Simulink. The results show that the adaptive non-singular terminal sliding mode control strategy based on the nonlinear disturbance observer proposed (PNDOANTSM) in this paper can reduce the average steady-state errors of robotic arm joints 1 and 2 by 36.58%, 38.40%, 44.68%, and 42.86%, compared with those observed in switching term adaptive law non-singular terminal sliding mode control based on a nonlinear disturbance observer (NDOANTSM) and non-singular terminal sliding mode control based on a nonlinear disturbance observer (NDONTSM). This paper provides a practical and feasible trajectory tracking control method for multi-joint robotic arms.

Keywords: robotic arm; nonlinear disturbance observer (NDO); non-singular terminal sliding mode (NTSM); adaptive control; trajectory tracking control

check for updates

Academic Editor: Chunhui Zhao

Received: 29 November 2024
Revised: 23 December 2024
Accepted: 15 January 2025
Published: 18 January 2025

Citation: Yin, S.; Shi, Z.; Liu, Y.; Xue, G.; You, H. Adaptive Non-Singular Terminal Sliding Mode Trajectory Tracking Control of Robotic Manipulators Based on Disturbance Observer Under Unknown Time-Varying Disturbance. *Processes* **2025**, *13*, 266. https://doi.org/10.3390/pr13010266

Copyright: © 2025 by the authors. Licensee MDPI, Basel, Switzerland. This article is an open access article distributed under the terms and conditions of the Creative Commons Attribution (CC BY) license (https://creativecommons.org/licenses/by/4.0/).

1. Introduction

The robotic arm can improve production efficiency and quality as a piece of high-performance automation equipment. The purpose of the trajectory tracking control of the robotic arm is so that it can quickly and accurately track the planned trajectory in complex

operation tasks by controlling its joint torque, such as by welding the specific position of the automobile body, uniformly spraying the body paint, and precisely assembling the automobile parts.

The robustness and dynamics of standard PID controllers are not ideal when they are affected by external disturbances. Therefore, scholars at home and abroad have proposed various types of control algorithms for robotic arms, such as neural network control [1–3], fuzzy control [4–6], sliding mode control (SMC) [7–10], reinforcement learning [11], robust control [12,13], iterative learning control [14], and model predictive control [15].

Among the above algorithms, Duan, J.G. et al. used radial basis function (RBF) neural networks to compensate for external disturbances and modeling errors [1]. Arefi, M.M. et al. combined adaptive algorithms with an RBF neural network to cope with stochastic uncertainty disturbances [2]. However, the neural network algorithm has the disadvantage of being computationally intensive and physically challenging to implement. Chen, J.Q. et al. proposed an improved super-twisted SMC algorithm based on adaptive fuzzy control for external perturbations and modeling errors. Fuzzy rules approximate the manipulator's uncertainty, and the adaptive law is utilized to modify and improve the fuzzy rules automatically [6]. However, the design of fuzzy rules requires extensive experience. Cao, S.J. et al. combined reinforcement learning and fixed-time SMC for manipulator control with unknown disturbances and actuator saturation. The designed controller performs fixed-time convergence for trajectory tracking errors [11]. However, the control method requires a large amount of training in advance and is difficult to apply in practical engineering. Busoniu, L. et al. indicated that reinforcement learning provides powerful algorithms for searching for optimal controllers for nonlinear systems with an unknown high degree of uncertainty, but the stability of reinforcement learning remains an open question for the most part [16].

Among the various methods, SMC has been widely used in robotic arm control due to its more straightforward physical implementation, robustness, and fast transient response. Conventional linear SMC can only guarantee an asymptotic convergence of states, indicating that high gains are required for fast convergence.

In contrast to conventional sliding modes, TSM control ensures the system converges in finite time. Yang, L. et al. proposed the concept of a non-singular fast terminal sliding mode (NFTSM) to avoid the singularity of the control process by taking advantage of the fast TSM [17]. Peng, L et al. proposed a fast non-singular integral TSM controller which introduces a power integral term containing a boundary-like structure. The specific contributions are twofold: firstly, this study posits that the singularity problem can be avoided without any constraints and provide a faster response, and secondly it shows that for constant or ultimately constant perturbations, we can ensure that there are zero steady-state errors when the boundary layer is used to mitigate chattering [18].

Zhang, L.Y. et al. improved robust tracking control for uncertain robotic arms. Approximate TSM control is proposed by combining a terminal sliding surface with a novel nonlinear function. Acceleration feedback for the lumped indeterminate part is no longer rquired, so the algebraic loop problem is completely avoided in the control law formulation. The transient tracking performance and steady-state tracking accuracy are further improved using the proposed smooth nonlinear function. This integrated design ensures fast transient and high-precision tracking accuracy [19].

Chen, W.H. et al. designed a nonlinear interference observer for the friction estimation and compensation of planar two-joint manipulators [20]. However, the nonlinear interference observer can only be used for planar manipulators with rotary joints. Mohammadi, A. et al. proposed an improved nonlinear perturbation observer independent of degrees of freedom, joint types, and robotic arm configurations for estimating system modeling

errors and external disturbances in response to the abovementioned problem. Finally, simulation experiments were conducted on a four-degree-of-freedom SCARA robotic arm to verify the algorithm's effectiveness [21]. Yang, J. et al. used an SMC method based on a nonlinear disturbance observer to estimate the external disturbances for an uncertain, unmatched system; the main contribution of this study is the design of a new sliding mode surface that introduces perturbation estimation directly into the SMC. This allows the state variables along the sliding mode surface to be driven to the equilibrium point. The numerical simulation results showed that the jitter suppression was superior to that under the linear SMC and integral I-SMC methods [22].

Neila, M.B.R. et al. state that to apply TSM control to robots, it is necessary to obtain precise upper bounds on the errors in the robot dynamics model and external disturbances beforehand. But because of the uncertainty and complexity of the parameters of the robot dynamics model, the interference upper bound is not easy to determine; a new adaptive TSM controller is therefore proposed to solve the trajectory tracking problem of the robot without the need to determine the interference upper bound in advance for this problem [23]. However, simulation experiments were conducted only on a planar two-degree-of-freedom robotic arm to verify the algorithm's effectiveness. Boukattaya, M. et al. proposed an adaptive NFTSM control algorithm for a case in which the upper bound of the system uncertainty is unknown. This adaptive method only requires the use of position and velocity measurements to estimate the upper bound of the system uncertainty [24]. Also, simulation experiments were carried out on a planar two-degree-of-freedom robotic arm, which verified the effectiveness of the algorithm. Yi, S.C. et al. introduced an adaptive technique for uncertainty compensation in response to external perturbations and inertial uncertainties and designed a second-order fast nonsingular TSM controller to eliminate jitter vibration [25]. Again, they used only a planar two-degree-of-freedom robotic arm for simulation to verify the effectiveness of the algorithm. Yang, Q.Y. et al. proposed an adaptive NFTSM control method, designed an adaptive updating law to compensate for the upper bound of the total set uncertainty, and verified the effectiveness of the proposed algorithm through the simulation of a planar two-degree-of-freedom robotic arm [26].

Susca, M. et al. addressed sampling rate optimization and execution time analysis for a two-degree-of-freedom control system. The optimization problem of sampling rate selection for this system is expressed in Equation, and a meta-analysis-based solution is proposed to find the optimal value of the sampling rate. This value provides a good trade-off between realizability and fidelity. An upper bound is estimated for the period required for all operations designed in the numerical implementation of the controller. A detailed analysis of the sampling rate and execution time is carried out for the end-to-end design process of the DC motor control problem [27]. Morar, D. et al. presented two approaches to the problem of cascade control of a two-axis position motor system. The first approach is to formulate a linear matrix inequality for the optimization problem to impose the positions of the closed-loop poles, taking into account the uncertainty of the system. The controller is a cascade structure consisting of a PI controller for the position loop and a P controller for the velocity loop, with additional feed-forward terms. The second approach is to design a cascade controller with an internal P-controller, and the external controller is a fractional-order controller [28].

In a study by Mobayen, S and Vu, M.T. et al., a fast terminal sliding mode control (FTSMC) method based on a disturbance observer is proposed to address the problem of underdriven robotic systems with sedation. The main innovation of the paper is that a disturbance observer-based FTSMC is designed. Using the disturbance observer to converge the disturbance approximation error in finite time, the effectiveness of the proposed

method is verified by simulation and experimentation on an actual cart-inverted bar [29]. Alattas, K.A. and Vu, M.T. et al. propose an adaptive NTSM control algorithm for perturbed nonlinear systems. A new nonlinear sliding surface is proposed based on the system's state. A barrier function adaptive scheme is designed to estimate the unknown perturbation upper limit. A nonlinear function is used in the sliding function to improve the control performance of the closed-loop system [30].

Tan, J. et al. address the problems in the time-triggered control of spacecraft. They design a new form of sliding mode surface by introducing particle filters. Dynamic and static ETMs associated with perturbation boundaries are constructed to ensure the asymptotic stability of the system under perturbation [31]. Lu, Y.T. et al. designed an improved twisted sliding mode control (ISTSMC) method for the control problem of electromagnetic direct-drive pumps by combining the HOSM convergence rate with a continuous function. An adaptive observer is designed for compensation, which is combined with ISTSMC to enhance the robustness of the system [32]. Sun, Y.H. et al. proposed a new event-triggered critical learning impedance controller for the impedance control of lower-limb exoskeleton robots. A critical architecture was designed. A modified gradient descent method with additional stability terms and historical and transient data were used to update the critic network. Continuous excitation conditions were relaxed. And the stability of the whole system was rigorously proved [33].

Mobayen, S and Vu, M.T. et al. address the problem in the fast calibration of nonlinear systems subjected to external perturbations. Combining an adaptive barrier function with TSM control allows the rapid convergence of the tracking error to zero. A priori knowledge of the external perturbation is no longer required, and the effectiveness of this is verified [34].

The advantages of NTSM algorithms, observers, and adaptive algorithms in the trajectory tracking control of robotic arms are well described in the above studies. However, there are still some shortcomings in the studies above that use only one or a combination of two of these algorithms. For the NTSM algorithm [35], strong robustness against uncertain dynamics and disturbances can be achieved if its switching gain is larger than the upper bound of uncertainty or disturbance. However, in practice, the upper bound of the disturbance is unknown, so the switching gain should be chosen to be large enough to cover a wide range of disturbances and uncertainties, such that a large switching gain may cause the jitter phenomenon leading to high-frequency oscillations in the system state. In other words, the above researchers used a combination of the NTSM algorithm and adaptive law to estimate the upper bound of interference, but if the upper bound of interference is too large, the switching gain will also rise, which will still cause jitter. Other researchers have used the NTSM algorithm and observer combination, using the observer to make an estimation of the system uncertainty and external interference, but there is interference error and there is still a need to switch the gain to cover the upper bound of the interference error. Furthermore, the switching gain is reduced, but there is still a need to determine the upper bound of the interference error using the system's a priori knowledge. Therefore, using one or both of the algorithms still comes with shortcomings.

In this paper, inspired by the above studies, a novel adaptive NTSM controller based on a nonlinear disturbance observer is proposed. It is used to track an N-link rigid robotic arm in the presence of system modeling errors and large external unknown time-varying disturbances.

The main contributions of this paper are as follows: (1) A a novel adaptive non-singular terminal sliding mode control method based on a nonlinear disturbance observer is proposed (PNDOANTSM) that is able to converge in finite time. (2) The improved NDO technique is used to observe the internal modeling error of the robotic arm and the

external unknown time-varying perturbations to which each joint is subjected for feed-forward compensation. Thus, the switching gain only needs to cover the perturbation observation error and not the total perturbation. This improves the robustness of the system. (3) In contrast to the usual need for a priori knowledge of the system uncertainty and disturbance boundaries, a set-total adaptive control law is designed to estimate the unknown uncertainty of the system without the need for a priori knowledge of upper bounds of the system uncertainty and external disturbances. (4) The s-term robustness adaptive law is triggered by introducing the observed perturbations and the size of the s-term norm error of the sliding mode surface. When an unknown large time-varying perturbation causes the sliding mode variable to move away from the sliding mode surface, the s-term coefficients are adaptively adjusted to converge to the sliding mode surface again to improve the robustness of the system.

The adaptive NTSM robotic arm trajectory tracking control algorithm based on the disturbance observer proposed in this paper is subjected to spatial two-degree-of-freedom robotic arm simulation to verify its effectiveness. The rest of this paper is organized as follows: In Section 2, a mathematical model of the robotic arm and the set perturbation boundary theorem are presented. In Section 3, the design process and stability analysis of the PNDOANTSM algorithmic controller are presented. In Section 4, the simulation results are presented. In Section 5, the main work of this paper is concluded.

2. Mathematical Model of Robotic Manipulators

According to the Lagrange method, the dynamic equations of the N-link robotic arm can be expressed as follows [36]:

$$M(q)\ddot{q} + C(q,\dot{q})\dot{q} + G(q) = \tau + \tau_d \tag{1}$$

where $q, \dot{q}, \ddot{q} \in R^n$ denotes the vector of joint positions, velocities, and accelerations of the robotic arm, $M(q) = M_0(q) + \Delta M(q)$ denotes the positive definite inertia matrix, $C(q,\dot{q}) = C_0(q,\dot{q}) + \Delta C(q,\dot{q})$ denotes the centripetal and Koch force matrix, $G(q) = G_0(q) + \Delta G(q)$ denotes the gravity matrix, τ denotes the joint input torque, and τ_d denotes the external interference torque. In this context, $M_0(q), C_0(q,\dot{q}), G_0(q)$ represents the nominal quantity, and $\Delta M(q), \Delta C(q,\dot{q}), \Delta G(q)$ represents the system modeling error. Therefore, system (1) can be expressed as follows:

$$M_0(q)\ddot{q} + C_0(q,\dot{q})\dot{q} + G_0(q) = \tau + F_d(q,\dot{q},\ddot{q}) \tag{2}$$

where $F_d(q,\dot{q},\ddot{q}) = \tau_d - \Delta M(q)\ddot{q} - \Delta C(q,\dot{q})\dot{q} - \Delta G(q)$ is the aggregate perturbation, representing the external disturbances to the system and the modeling errors within the system.

The objective of this paper is to design a controller capable of achieving highly accurate trajectory tracking in the presence of unknown time-varying disturbances. In order to achieve this goal, the following assumptions need to be made about the system (2).

Assumption 1. *The inertia matrix remains $M_0(q)$ bounded for all joint angles q, even with uncertainty.*

Assumption 2. *The lumped disturbance $F_d(q,\dot{q},\ddot{q})$ is bounded by the following:*

$$\| F_d(q,\dot{q},\ddot{q}) \| < b_0 + b_1 \| q \| + b_2 \| \dot{q} \|^2 \tag{3}$$

where b_0, b_1, b_2 are unknown positive constants and $\| \cdot \|$ denotes the Euclidean norm of the vector.

Remark 1. *The above assumptions are reasonable based on the characteristics of industrial robot manipulators, e.g., [24,37,38]. The literature [23] states that a system's uncertainty is related to*

the control input and that if the control input does not contain an acceleration signal, the system uncertainty will be bounded by a positive function of the position and velocity measurements. Several researchers have used this bounded property [24,25].

3. PNDOANTSM Controller Design

Set $q_d, \dot{q}_d, \ddot{q}_d$, as the desired position, velocity, and acceleration of the robotic arm joints, and $q, \dot{q}, \ddot{q}$, as the actual output position, velocity, and acceleration of the robotic arm joints. The trajectory tracking error of the robotic arm and its derivatives are shown in Equations (4)–(6):

$$e = q - q_d \tag{4}$$

$$\dot{e} = \dot{q} - \dot{q}_d \tag{5}$$

$$\ddot{e} = \ddot{q} - \ddot{q}_d \tag{6}$$

In this paper, the state variables ε_1, and ε_2 are constructed based on the position e, velocity $\dot{e}$ and acceleration $\ddot{e}$ errors of the robotic arm joints, where $\varepsilon_1 = e, \varepsilon_2 = \dot{\varepsilon}_1 = \dot{e}, \dot{\varepsilon}_2 = \ddot{e}$.

Taking the state variables of error $\varepsilon_1 = e, \varepsilon_2 = \dot{\varepsilon}_1 = \dot{e}, \dot{\varepsilon}_2 = \ddot{e}$, introducing Equation (2) into Equation (6), the equation of error dynamics of the robotic arm can be written as follows:

$$\begin{aligned} \dot{\varepsilon}_1 &= \varepsilon_2 \\ \dot{\varepsilon}_2 &= M_0^{-1}(q)(\tau - (C_0(q,\dot{q})\dot{q} + G_0(q)) + F_d(q,\dot{q},\ddot{q})) - \ddot{q}_d \end{aligned} \tag{7}$$

Let $F_N(q,\dot{q},\ddot{q}) = M_0^{-1}(q)F_d(q,\dot{q},\ddot{q})$; according to Assumptions 1 and 2, the following can be obtained:

$$\| F_N(q,\dot{q},\ddot{q}) \| < b_0 + b_1 \| q \| + b_2 \| \dot{q} \|^2 \tag{8}$$

where b_0, b_1 and b_2 are unknown positive constants.

3.1. Design of Nonlinear Disturbance Observer

In order to estimate the aggregate perturbation $F_d(q,\dot{q},\ddot{q})$ of the system, the following nonlinear perturbation observer is designed in conjunction with Equation (2):

$$\begin{aligned} \dot{z} &= -L(q,\dot{q})\hat{F}_d(q,\dot{q},\ddot{q}) + L(q,\dot{q})[C_0(q,\dot{q})\dot{q} + G_0(q) - \tau] \\ \hat{F}_d(q,\dot{q},\ddot{q}) &= z + p(q,\dot{q}) \\ p(q,\dot{q}) &= L(q,\dot{q})M_0(q)\ddot{q} \end{aligned} \tag{9}$$

where z is the defined auxiliary variable, $L(q,\dot{q})$ is the gain matrix of the observer, which determines the auxiliary vector $p(q,\dot{q})$ of the observer, and $\hat{F}_d$ is the observed value of the total system perturbations. According to the article [20], $L(q,\dot{q})$ and $p(q,\dot{q})$ can be designed as follows:

$$\begin{aligned} L(q,\dot{q}) &= X^{-1}M_0^{-1}(q) \\ p(q,\dot{q}) &= X^{-1}\dot{q} \end{aligned} \tag{10}$$

where X is a constant invertible matrix and the inertia matrix $M_0(q)$ is a symmetric positive definite matrix. X is found by a linear matrix inequality. Define $\widetilde{F}_d(q,\dot{q},\ddot{q}) = F_d(q,\dot{q},\ddot{q}) - \hat{F}_d(q,\dot{q},\ddot{q})$ as the disturbance observation error. In this paper, the above symbols are abbreviated. For example, $F_d(q,\dot{q},\ddot{q}) = F_d$. Equation (11) can be derived from the observer, as shown in Equation (9):

$$\begin{aligned}\dot{\tilde{F}}_d &= \dot{F}_d - \dot{\hat{F}}_d \\ &= \dot{F}_d - \dot{z} - \dot{p} \\ &= \dot{F}_d - L[C_0\dot{q} + G_0 - \tau] + L\hat{F}_d - LM_0\ddot{q} \\ &= \dot{F}_d + L\hat{F}_d - L[M_0\ddot{q} + C_0\dot{q} + G_0 - \tau] \\ &= \dot{F}_d + L\hat{F}_d - LF_d \\ &= \dot{F}_d - L\tilde{F}_d\end{aligned} \tag{11}$$

There is generally no differential priori knowledge of disturbance $F_d(q, \dot{q}, \ddot{q})$. Assuming that the change in the dynamic properties of the disturbance is slow with respect to the observer [19], $\dot{F}_d = 0$ can be set. Further, the error equations of the observer can be denoted as in Equations (12) and (13):

$$\dot{\tilde{F}}_d = -L\tilde{F}_d = -X^{-1}M_0^{-1}\tilde{F}_d \tag{12}$$

$$\dot{\tilde{F}}_d^{\,T} = -(X^{-1}M_0^{-1}\tilde{F}_d X^T = -\tilde{F}_d^T M_0^{-T} X^{-T} \tag{13}$$

Design the Lyapunov function as follows:

$$V_0 = \tilde{F}_d^T X^T M_0 X \tilde{F}_d \tag{14}$$

The derivative of the above Lyapunov function is as follows:

$$\dot{V}_0 = \dot{\tilde{F}}_d^{\,T} X^T M_0 X \tilde{F}_d + \tilde{F}_d^T X^T \dot{M}_0 X \tilde{F}_d + \tilde{F}_d^T X^T M_0 X \dot{\tilde{F}}_d \tag{15}$$

Substituting Equations (12) and (13) into Equation (15) yields the following:

$$\begin{aligned}\dot{V}_0 &= \dot{\tilde{F}}_d^{\,T} X^T M_0 X \tilde{F}_d + \tilde{F}_d^T X^T \dot{M}_0 X \tilde{F}_d + \tilde{F}_d^T X^T M_0 X \dot{\tilde{F}}_d \\ &= -\tilde{F}_d^T M_0^{-T} X^{-T} X^T M_0 X \tilde{F}_d + \tilde{F}_d^T X^T \dot{M}_0 X \tilde{F}_d - \tilde{F}_d^T X^T M_0 X X^{-1} M_0^{-1} \tilde{F}_d \\ &= -\tilde{F}_d^T X \tilde{F}_d + \tilde{F}_d^T X^T \dot{M}_0 X \tilde{F}_d - \tilde{F}_d^T X^T \tilde{F}_d \\ &= -\tilde{F}_d^T (X - X^T \dot{M}_0 X + X^T) \tilde{F}_d\end{aligned} \tag{16}$$

Constructing the inequality, we can obtain the following:

$$X + X^T - X^T \dot{M}_0 X \geq \varphi \tag{17}$$

where $\varphi > 0$, φ is a symmetric positive definite matrix. Then, there exists φ', which leads to Equation (18).

$$\dot{V}_0 \leq -\tilde{F}_d^T \varphi \tilde{F}_d = -\varphi' V_0 \tag{18}$$

where $\varphi' > 0$; it can be seen that the NDO converges exponentially [20].

The above equation, Equation (17), is transformed into a linear matrix inequality to be solved, defining the matrix X.

The linear matrix inequality is as follows:

$$\begin{bmatrix} Y + Y^T - \omega I & Y^T \\ Y & \varphi^{-1} \end{bmatrix} \geq 0 \tag{19}$$

After obtaining the X^{-1} matrix, the observation gain matrix $L(q, \dot{q})$ and the auxiliary variables $p(q, \dot{q})$ can be derived.

3.2. Design of Adaptive Non-Singular Terminal Sliding Mode Controller

Next, we design an adaptive terminal sliding mode controller (ANTSM) for the system to estimate the system uncertainty and the unknown upper limit of the disturbance, considering that when the robotic arm suddenly encounters an unknown large-value perturbation, adjusting the $sign(.)$ symbol term gain only by the adaptive switching control law causes chattering when the term switching gain is too large. At the same time, the robust term adaptive control law is introduced to adjust the s-term gain coefficient, which can ensure fast convergence and weaken chattering at the same time. Firstly, the NTSM surface is introduced [28]:

$$s = \varepsilon_1 + \frac{1}{\beta}|\varepsilon_2|^{\frac{p}{r}} sign(\varepsilon_2) \tag{20}$$

where $\beta > 0, p, r$ are positive odd numbers and $1 < p/r < 2$, $sign(.)$ is the sign function. The derivative of Equation (20) concerning time is as follows:

$$\dot{s} = \varepsilon_2 + \frac{1}{\beta}\frac{p}{r}|\varepsilon_2|^{\frac{p}{r}-1}\dot{\varepsilon}_2 \tag{21}$$

The control law τ of the robotic arm consists of the equivalent control law τ_{eq} and the adaptive switching control law τ_{asw}, and the current control law can be designed as shown in Equations (22)–(24):

$$\tau = \tau_{eq} + \tau_{asw} \tag{22}$$

$$\tau_{\mathrm{eq}} = M_0\ddot{q}_d + C_0\dot{q} + G_0 - \beta\frac{r}{p}|\varepsilon_2|^{2-\frac{p}{r}} sign(\varepsilon_2) \tag{23}$$

$$\begin{array}{ll} \tau_{\mathrm{asw}} & = -M_0(\mathrm{k}_1 s + \mathrm{k}_2 sign(s)) \\ \mathrm{k}_1 & = \mathrm{k}_0(1 + \hat{a}_0) \\ \mathrm{k}_2 & = \hat{b}_0 + \hat{b}_1 \parallel q \parallel + \hat{b}_2 \parallel \dot{q} \parallel^2 \end{array} \tag{24}$$

where k_0 is a positive definite gain matrix, $\hat{a}_0, \hat{\mathrm{b}}_0, \hat{\mathrm{b}}_1, \hat{\mathrm{b}}_2$ are estimates of $a_0, \mathrm{b}_0, \mathrm{b}_1, \mathrm{b}_2$ and $a_0, \mathrm{b}_0, \mathrm{b}_1, \mathrm{b}_2$ are unknown positive numbers. In fact, because of the measurement error and switching delay of the system, $\parallel s \parallel$ cannot always be exactly zero, so the adaptive parameter may increase slowly and infinitely. In order to overcome this drawback, the dead zone technique is used for designing the adaptive law, and for the robust term adaptive law, the disturbance observed by the introduction of a disturbance observer is used in conjunction with the sliding mode error to determine whether to regulate the robust gain coefficients of the s term or not. The parameters $\hat{a}_0, \hat{\mathrm{b}}_0, \hat{\mathrm{b}}_1, \hat{\mathrm{b}}_2$ are updated by the following adaptive laws.

$$\begin{array}{l} \dot{\hat{a}}_0 = \begin{cases} H_0 \parallel s \parallel^2 |\varepsilon_2|^{\frac{p}{r}-1}, \text{if} \parallel s \parallel \geq \xi \cap \parallel \hat{F}_d \parallel \geq \gamma \\ 0, \text{if} \parallel s \parallel < \xi \end{cases} \\ \dot{\hat{b}}_0 = \begin{cases} \lambda_0 \parallel s \parallel |\varepsilon_2|^{\frac{p}{r}-1}, \text{if} \parallel s \parallel \geq \xi \\ 0, \text{if} \parallel s \parallel < \xi \end{cases} \\ \dot{\hat{b}}_1 = \begin{cases} \lambda_1 \parallel s \parallel \parallel q \parallel |\varepsilon_2|^{\frac{p}{r}-1}, \text{if} \parallel s \parallel \geq \xi \\ 0, \text{if} \parallel s \parallel < \xi \end{cases} \\ \dot{\hat{b}}_2 = \begin{cases} \lambda_2 \parallel s \parallel \parallel q \parallel^2 |\varepsilon_2|^{\frac{p}{r}-1}, \text{if} \parallel s \parallel \geq \xi \\ 0, \text{if} \parallel s \parallel < \xi \end{cases} \end{array} \tag{25}$$

where $\lambda_0, \lambda_1, \lambda_2$ and H_0 are arbitrary positive numbers representing the tuning parameters. ξ is a very small positive number that limits the slow and infinite increase in the adaptive parameter by setting the deadband range, and γ is a positive number that is used to set the trigger conditions for the robust adaptive law, which is beyond the numerical bounds of the deadband range and the observed perturbation.

3.3. PNDOANTSM Controller Design and Stability Analysis

In this paper, the disturbance is observed by introducing a nonlinear disturbance observer, and the control law after adding the disturbance observer compensation is as follows:

$$\begin{aligned} \tau = & \quad \tau_{\text{eq}} + \tau_{\text{asw}} - \hat{F}_d \\ = & \quad M_0\ddot{q}_d + C_0\dot{q} + G_0 - \beta\frac{r}{p}|\varepsilon_2|^{2-\frac{p}{r}}sign(\varepsilon_2) \\ & -M_0(\mathrm{k}_0(1+\hat{a}_0)s + (\hat{b}_0 + \hat{b}_1 \parallel q \parallel + \hat{b}_2 \parallel \dot{q} \parallel^2)sign(s)) - \hat{F}_d \end{aligned} \tag{26}$$

Among them, the s term robust adaptive law and the $sign()$ term switching adaptive law are shown in Equation (25). A schematic diagram of the control system discussed in this paper is shown in Figure 1.

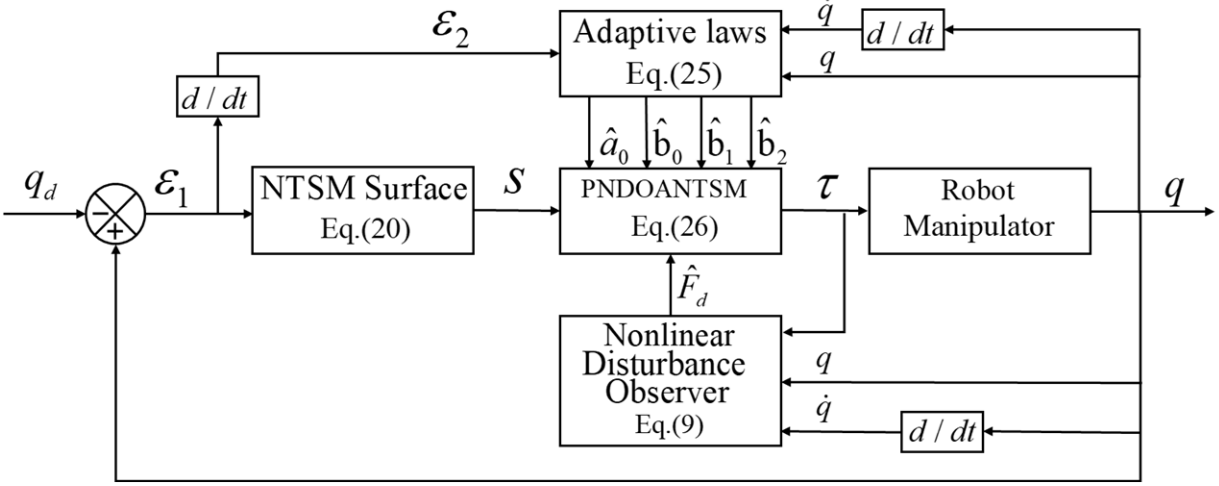


Figure 1. Schematic diagram of the control system for the PNDOANTSM algorithm.

In control system stability analysis, we consider the following Lyapunov function:

$$V_1 = \frac{1}{2}s^Ts + \frac{1}{\beta}\frac{p}{r}\frac{\mathrm{k}_0}{2H_0}(\hat{a}_0 - a_0)^2 + \frac{1}{\beta}\frac{p}{r}\sum_{i=0}^{2}\frac{1}{2\lambda_i}\left(\hat{b}_i - b_i\right)^2 + \tilde{F}_d^T X^T M_0 X\tilde{F}_d \tag{27}$$

Substituting Equation (14) into Equation (27), the derivative of V_1 with respect to time is obtained as shown in Equation (28):

$$\dot{V}_1 = s^T\dot{s} + \frac{1}{\beta}\frac{p}{r}\frac{\mathrm{k}_0}{H_0}(\hat{a}_0 - a_0)\dot{\hat{a}}_0 + \frac{1}{\beta}\frac{p}{r}\sum_{i=0}^{2}\frac{1}{\lambda_i}\left(\hat{b}_i - b_i\right)\dot{\hat{b}}_i + \dot{V}_0 \tag{28}$$

Substituting Equations (7) and (21) into Equation (28) yields Equation (29):

$$\begin{aligned} \dot{V}_1 = & s^T(\varepsilon_2 + \frac{1}{\beta}\frac{p}{r}|\varepsilon_2|^{\frac{p}{r}-1}(M_0^{-1}(\tau - (C_0\dot{q} + G_0) + F_d) - \ddot{q}_d)) \\ & + \frac{1}{\beta}\frac{p}{r}\frac{\mathrm{k}_0}{H_0}(\hat{a}_0 - a_0)\dot{\hat{a}}_0 + \frac{1}{\beta}\frac{p}{r}\sum_{i=0}^{2}\frac{1}{\lambda_i}\left(\hat{b}_i - b_i\right)\dot{\hat{b}}_i + \dot{V}_0 \end{aligned} \tag{29}$$

Substituting the control law equation, Equation (26), into Equation (29) yields Equation (30):

$$\begin{aligned}\dot{V}_1 = \quad & s^T(\frac{1}{\beta}\frac{p}{r}|\varepsilon_2|^{\frac{p}{r}-1}(-\mathrm{k}_0(1+\hat{a}_0)s-(\hat{b}_0+\hat{b}_1 \parallel q \parallel +\hat{b}_2 \parallel \dot{q} \parallel^2)sign(\mathrm{s})+M_0^{-1}(F_d-\hat{F}_d))) \\ & +\frac{1}{\beta}\frac{p}{r}\frac{\mathrm{k}_0}{H_0}(\hat{a}_0-a_0)\dot{\hat{a}}_0+\frac{1}{\beta}\frac{p}{r}\sum_{i=0}^{2}\frac{1}{\lambda_i}\left(\hat{b}_i-b_i\right)\dot{\hat{b}}_i+\dot{V}_0 \\ = \quad & \frac{1}{\beta}\frac{p}{r}|\varepsilon_2|^{\frac{p}{r}-1}(-\mathrm{k}_0 s^2-\mathrm{k}_0\hat{a}_0 s^2-(\hat{b}_0+\hat{b}_1 \parallel q \parallel +\hat{b}_2 \parallel \dot{q} \parallel^2) \parallel s \parallel +sM_0^{-1}\widetilde{F}_d) \\ & +\frac{1}{\beta}\frac{p}{r}\frac{\mathrm{k}_0}{H_0}(\hat{a}_0-a_0)\dot{\hat{a}}_0+\frac{1}{\beta}\frac{p}{r}\sum_{i=0}^{2}\frac{1}{\lambda_i}\left(\hat{b}_i-b_i\right)\dot{\hat{b}}_i+\dot{V}_0\end{aligned} \tag{30}$$

Substituting the adaptive parameter update law equation, Equation (25), and the observer error equation, Equation (12), into Equation (30) yields Equation (31):

$$\begin{aligned}\dot{V}_1 = \quad & \tfrac{1}{\beta}\tfrac{p}{r}|\varepsilon_2|^{\frac{p}{r}-1}(-\mathrm{k}_0 s^2-\mathrm{k}_0\hat{a}_0 s^2-(\hat{b}_0+\hat{b}_1 \parallel q \parallel +\hat{b}_2 \parallel \dot{q} \parallel^2) \parallel s \parallel +sM_0^{-1}\widetilde{F}_d) \\ & +\tfrac{1}{\beta}\tfrac{p}{r}\mathrm{k}_0(\hat{a}_0-a_0) \parallel s \parallel^2 |\varepsilon_2|^{\frac{p}{r}-1}+\tfrac{1}{\beta}\tfrac{p}{r}\left(\hat{b}_0-b_0\right) \parallel s \parallel |\varepsilon_2|^{\frac{p}{r}-1} \\ & +\tfrac{1}{\beta}\tfrac{p}{r}\left(\hat{b}_1-b_1\right) \parallel s \parallel |\varepsilon_2|^{\frac{p}{r}-1} \parallel q \parallel +\tfrac{1}{\beta}\tfrac{p}{r}\left(\hat{b}_2-b_2\right) \parallel s \parallel |\varepsilon_2|^{\frac{p}{r}-1} \parallel \dot{q} \parallel^2 \\ & +\dot{V}_0 \\ = \quad & \tfrac{1}{\beta}\tfrac{p}{r}|\varepsilon_2|^{\frac{p}{r}-1}(-\mathrm{k}_0 s^2-\mathrm{k}_0 a_0 s^2-(b_0+b_1 \parallel q \parallel +b_2 \parallel \dot{q} \parallel^2) \parallel s \parallel +sM_0^{-1}\widetilde{F}_d) \\ & +\dot{V}_0\end{aligned} \tag{31}$$

After the introduction of disturbance compensation, the total set disturbances F_d are changed from disturbance errors $\widetilde{F}_d$, so the total set disturbances are updated as shown in Equation (32):

$$F_N = M_0^{-1}\widetilde{F}_d \tag{32}$$

Substituting the updated obtained set-total disturbance F_N into Equation (31) yields the following:

$$\begin{aligned}\dot{V}_1 \quad & = \tfrac{1}{\beta}\tfrac{p}{r}|\varepsilon_2|^{\frac{p}{r}-1}(-\mathrm{k}_0 s^2-\mathrm{k}_0 a_0 s^2-(b_0+b_1 \parallel q \parallel +b_2 \parallel \dot{q} \parallel^2) \parallel s \parallel +sF_N)+\dot{V}_0 \\ & = \tfrac{1}{\beta}\tfrac{p}{r}|\varepsilon_2|^{\frac{p}{r}-1}(-\mathrm{k}_0 s^2-\mathrm{k}_0 a_0 s^2-(b_0+b_1 \parallel q \parallel +b_2 \parallel \dot{q} \parallel^2-F_N) \parallel s \parallel)+\dot{V}_0\end{aligned} \tag{33}$$

From Equation (8), $\parallel F_N(q,\dot{q},\ddot{q}) \parallel < b_0+b_1 \parallel q \parallel +b_2 \parallel \dot{q} \parallel^2$ and from Equation (18), $\dot{V}_0 \le -\widetilde{F}_d^T\varphi\widetilde{F}_d = -\varphi' V_0$, where k_0, a_0, and φ' are positive numbers. Therefore, applying Equations (8) and (18) and introducing Equation (33) yields the following:

$$\begin{aligned}\dot{V}_1 \quad & \le \tfrac{1}{\beta}\tfrac{p}{r}|\varepsilon_2|^{\frac{p}{r}-1}(-\mathrm{k}_0 s^2-\mathrm{k}_0 a_0 s^2-(b_0+b_1 \parallel q \parallel +b_2 \parallel \dot{q} \parallel^2-F_N) \parallel s \parallel)-\varphi' V_0 \\ & \le \tfrac{1}{\beta}\tfrac{p}{r}|\varepsilon_2|^{\frac{p}{r}-1}(-\mathrm{k}_0 s^2-\mathrm{k}_0 a_0 s^2)-\varphi' V_0 \\ & \le -\tfrac{1}{\beta}\tfrac{p}{r}|\varepsilon_2|^{\frac{p}{r}-1}\mathrm{k}_0 s^2 \le 0\end{aligned} \tag{34}$$

According to Lyapunov stability theory, the state of the system converges asymptotically to the sliding surface $s(t) = 0$.

To prove that the asymptotic convergence of the system state to the sliding surface occurs in finite time, we can consider the following Lyapunov function candidate:

$$V_2 = \frac{1}{2}s^T s \tag{35}$$

Differentiating V_2 with respect to time yields the following:

$$\dot{V}_2 = s^T\dot{s} \tag{36}$$

Substituting Equations (18) and (28) into Equation (36) yields the following:

$$\begin{aligned}\dot{V}_2 &= \dot{V}_1 - \frac{1}{\beta}\frac{p}{r}\frac{\mathrm{k}_0}{H_0}(\hat{a}_0 - a_0)\dot{\hat{a}}_0 - \frac{1}{\beta}\frac{p}{r}\sum_{i=0}^{2}\frac{1}{\lambda_i}\left(\hat{b}_i - b_i\right)\dot{\hat{b}}_i - \dot{V}_0 \\ &\leq -\frac{1}{\beta}\frac{p}{r}|\varepsilon_2|^{\frac{p}{r}-1}\mathrm{k}_0 s^2 - \frac{1}{\beta}\frac{p}{r}\frac{\mathrm{k}_0}{H_0}(\hat{a}_0 - a_0)\dot{\hat{a}}_0 - \frac{1}{\beta}\frac{p}{r}\sum_{i=0}^{2}\frac{1}{\lambda_i}\left(\hat{b}_i - b_i\right)\dot{\hat{b}}_i - \varphi' V_0 \ . \\ &\leq -\frac{1}{\beta}\frac{p}{r}|\varepsilon_2|^{\frac{p}{r}-1}\mathrm{k}_0 s^2 - \frac{1}{\beta}\frac{p}{r}\frac{\mathrm{k}_0}{H_0}(\hat{a}_0 - a_0)\dot{\hat{a}}_0 - \frac{1}{\beta}\frac{p}{r}\sum_{i=0}^{2}\frac{1}{\lambda_i}\left(\hat{b}_i - b_i\right)\dot{\hat{b}}_i\end{aligned} \tag{37}$$

For ease of analysis, let $c_0 = a_0, c_1 = b_0, c_2 = b_1, c_3 = b_2$; then, $\hat{c}_0 = \hat{a}_0, \hat{c}_1 = \hat{b}_0, \hat{c}_2 = \hat{b}_1, \hat{c}_3 = \hat{b}_2$.

Case 1: When $\hat{c}_i(0) < c_i, i = 0, 1, 2, 3$, the analysis consists of two steps.

Step 1: With the aid of $\dot{\hat{c}}_i \geq 0$, suppose that there is finite time $T_1 \geq 0$, such that all $\hat{c}_i(t) \geq c_i, t \geq T_1$, which gives rise to $\dot{V}_2 \leq -\frac{1}{\beta}\frac{p}{r}|\varepsilon_2|^{\frac{p}{r}-1}\mathrm{k}_0 s^2, t \geq T_1$.

Step 2: Otherwise, there exists another finite time T_2, such that at least one of $\dot{\hat{c}}_i = 0$ and $\hat{c}_i(t) < c_i, t \geq T_2$ applies. Without a loss of generality, assume that $\dot{\hat{c}}_i = 0$ and $\hat{c}_i(t) < c_i, i = 2, 3, t \geq T_2$, which yields $\dot{V}_2 \leq -\frac{1}{\beta}\frac{p}{r}|\varepsilon_2|^{\frac{p}{r}-1}\mathrm{k}_0 s^2 - \frac{1}{\beta}\frac{p}{r}\frac{\mathrm{k}_0}{H_0}(\hat{a}_0 - a_0)\dot{\hat{a}}_0 - \frac{1}{\beta}\frac{p}{r}\frac{1}{\lambda_0}\left(\hat{b}_0 - b_0\right)\dot{\hat{b}}_0, t \geq T_2$. As for c_0 and c_1, the analysis is the same as that in Step 1 or Step 2. Therefore, we can obtain $\dot{V}_2 \leq -\frac{1}{\beta}\frac{p}{r}|\varepsilon_2|^{\frac{p}{r}-1}\mathrm{k}_0 s^2$ in a finite time T_3.

Case 2: When at least one of $\hat{c}_i(0) > c_i, i = 0, 1, 2, 3$, one has $\hat{c}_i(0) > c_i, t \geq 0$, that is, $-(\hat{c}_i - c_i)\dot{\hat{c}}_i \leq 0$. As for $\hat{c}_j(0) < c_j, j \neq i$, similarly to what is observed in the analysis of Case 1, $\dot{V}_2 \leq -\frac{1}{\beta}\frac{p}{r}|\varepsilon_2|^{\frac{p}{r}-1}\mathrm{k}_0 s^2$ is yielded in finite time; thus, the finite time convergence of s can be guaranteed.

From Case 1 and Case 2, for any initial condition $(s(0), \hat{c}_i(0))$, there always exists a positive number $\frac{2}{\beta}\frac{p}{r}|\varepsilon_2|^{\frac{p}{r}-1}\mathrm{k}_0$ and a finite time constant T, such that we can observe the following:

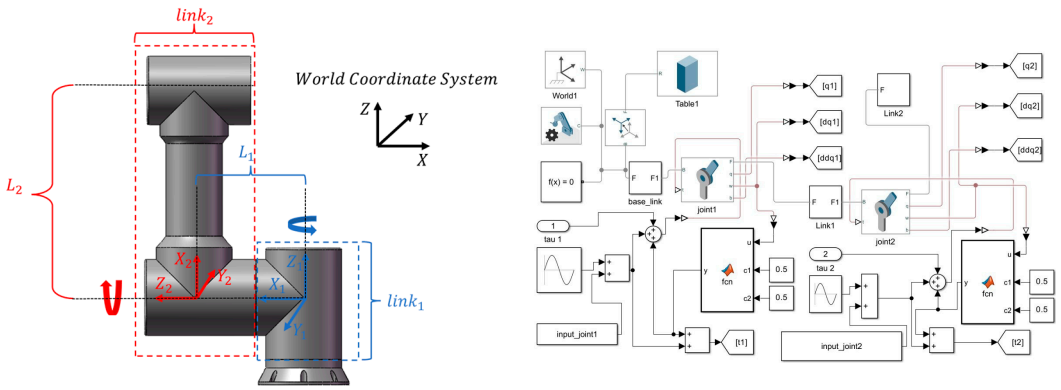
$$\dot{V}_2(t) \leq -\frac{1}{\beta}\frac{p}{r}|\varepsilon_2|^{\frac{p}{r}-1}\mathrm{k}_0 s^2 \leq -\frac{2}{\beta}\frac{p}{r}|\varepsilon_2|^{\frac{p}{r}-1}\mathrm{k}_0 V_2, t \geq T \tag{38}$$

Hence, according to the Lyapunov stability criterion, the PNDOANTSM manifold $s = 0$ can be established in finite time. This completes the proof.

4. Simulation Studies

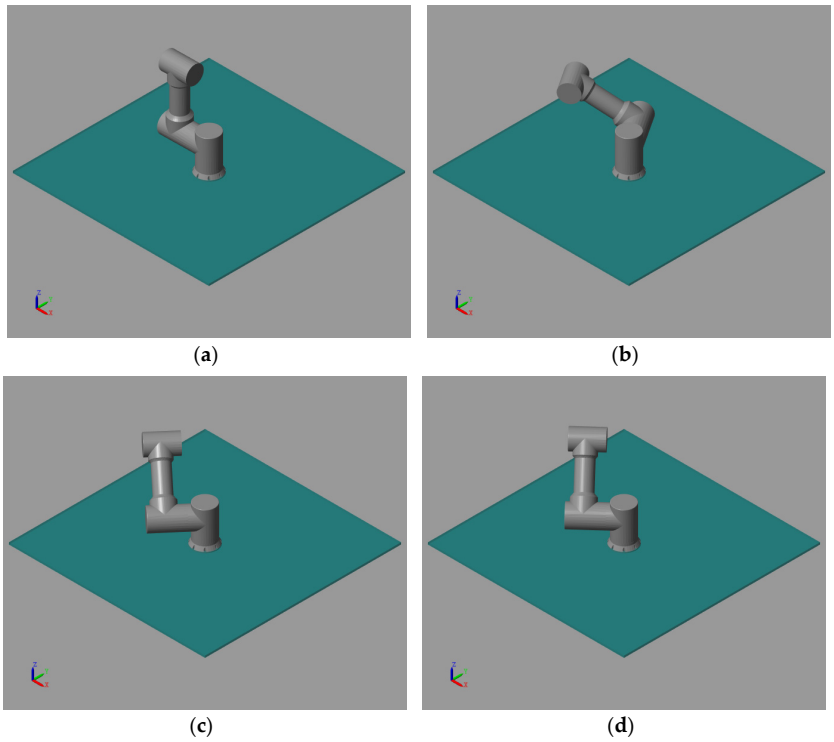
The recommended workstation configuration and simulation environment information for this study is as follows: operating system, Windows 10; processor, intel(R) Core(TM) i7-7700 CPU @ 3.60 GHz; RAM, 32.0 GB; 64-bit operating system; simulation software, MATLAB, Version: R2023b. We also used the Simulink environment and Simscape toolbox in MATLAB. The development code is in MATLAB language.

In this section, to verify the effectiveness and reliability of the control algorithm of the robotic manipulators proposed in this paper, a space two-joint robotic arm is used for simulation verification, and the robotic manipulator model is shown in Figure 2a. The Simulink and Simscape toolboxes are used to build a simulation model of the controlled object of the spatial two-link robotic manipulators, as shown in Figure 2b. The simulation visualization of a two-link robotic arm in space is shown in Figure 3. Simulation is carried out to verify the effectiveness of the proposed control algorithm. The simulation model of the designed trajectory tracking control algorithm of the robotic manipulators is shown in Figure 4.



(**a**) (**b**)

Figure 2. (**a**) Configuration of a space two-link robotic manipulator. (**b**) Simscape-constructed two-link robotic manipulators in space.



(**a**) (**b**)

(**c**) (**d**)

Figure 3. Simulated visualization of a two-link robotic arm in space. (**a**) The 0th second moment; (**b**) 5th second moment; (**c**) 15th second moment; (**d**) 20th second moment.

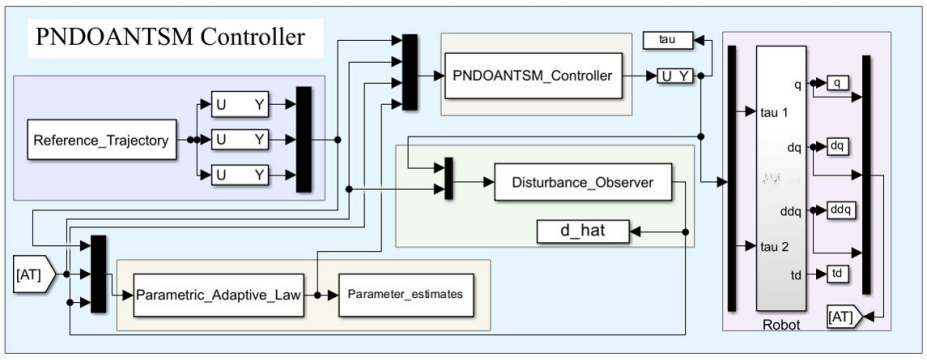


Figure 4. Robotic manipulator simulation model.

The dynamical equations of a spatial two-link robotic manipulator system are as follows [39]:

$$\begin{bmatrix} M_{11}(q) & M_{12}(q) \\ M_{21}(q) & M_{22}(q) \end{bmatrix} \begin{bmatrix} \ddot{q}_1 \\ \ddot{q}_2 \end{bmatrix} + \begin{bmatrix} C_{11}(q,\dot{q}) & C_{12}(q,\dot{q}) \\ C_{21}(q,\dot{q}) & C_{22}(q,\dot{q}) \end{bmatrix} \begin{bmatrix} \dot{q}_1 \\ \dot{q}_2 \end{bmatrix} + \begin{bmatrix} G_1(q) \\ G_2(q) \end{bmatrix} = \begin{bmatrix} \tau_1 \\ \tau_2 \end{bmatrix} + \begin{bmatrix} \tau_{d1} \\ \tau_{d2} \end{bmatrix} \quad (39)$$

$$\begin{aligned} M_{11}(q) &= J_{1zz} + m_1 l_1^2 + m_2 L_1^2 + \left(J_{2yy} + m_2 l_2^2\right) \times \sin^2(q_2) + J_{2xx} \cos^2(q_2) \\ M_{12}(q) &= -m_2 L_1 l_2 \cos(q_2) \\ M_{21}(q) &= -m_2 L_1 l_2 \cos(q_2) \\ M_{22}(q) &= J_{2zz} + m_2 l_2^2 \\ C_{11}(q,\dot{q}) &= \tfrac{1}{2} \times \left(m_2 l_2^2 + J_{2yy} - J_{2xx}\right) \times \dot{q}_2 \times \sin(2q_2) \\ C_{12}(q,\dot{q}) &= \tfrac{1}{2} \times \left(m_2 l_2^2 + J_{2yy} - J_{2xx}\right) \times \dot{q}_1 \times \sin(2q_2) + m_2 L_1 l_2 \times \dot{q}_2 \times \sin(q_2) \\ C_{21}(q,\dot{q}) &= -\tfrac{1}{2} \times \left(m_2 l_2^2 + J_{2yy} - J_{2xx}\right) \times \dot{q}_1 \times \sin(2q_2) \\ C_{22}(q,\dot{q}) &= 0 \\ G_1(q) &= 0 \\ G_2(q) &= -m_2 g l_2 \sin(q_2) \end{aligned} \quad (40)$$

where L_1, L_2 are the lengths of links 1 and 2, l_1, l_2 are the distances from the center of mass of each link to the origin of its link coordinate system, m_1, m_2 are the masses of links 1 and 2, J_1, J_2 are the inertia tensor matrices of links 1 and 2, τ_1, τ_2 are the input torques of joints 1 and 2, τ_{d1}, τ_{d2} are the external perturbations of joints 1 and 2, and g is the gravitational acceleration, where the inertia tensor matrix is of the following form:

$$J_1 = \begin{bmatrix} J_{1xx} & 0 & 0 \\ 0 & J_{1yy} & 0 \\ 0 & 0 & J_{1zz} \end{bmatrix}, J_2 = \begin{bmatrix} J_{2xx} & 0 & 0 \\ 0 & J_{2yy} & 0 \\ 0 & 0 & J_{2zz} \end{bmatrix} \quad (41)$$

The reference trajectory of the spatial two-jointed robotic manipulator is chosen as follows.

$$q_d = \begin{bmatrix} q_{1d} \\ q_{2d} \end{bmatrix} = \begin{bmatrix} \sin\left(t - \frac{\pi}{8}\right) \\ \sin\left(t - \frac{\pi}{8}\right) \end{bmatrix} \quad (42)$$

The initial joint angles of the spatial two-jointed robotic manipulator are $q_1(0) = 0(rad), q_2(0) = 0(rad)$, and the initial desired joint angle positions are $q_{1d}(0) = 0.3827(rad), q_{2d}(0) = 0.3827(rad)$. The physical parameters of the spatial two-jointed robotic manipulator are given in Table 1.

Table 1. Physical parameters of the space two-link robotic manipulator.

Symbol	Definition	Value
m_1	Mass of Link 1	2.79 kg
m_2	Mass of Link 2	6.42 kg
L_1	Length of Link 1	0.1470 m
l_1	Distance from the Center of Gravity of Link 1	0.0063 m
l_2	Distance from the Center of Gravity of Link 2	0.1251 m
$J_{1xx}, J_{1yy}, J_{1zz}$	Inertia Moment of Link 1 Computed with Respect to its Center of Mass;	0.006645 kg·m^2 0.007162 kg·m^2 0.004328 kg·m^2
$J_{2xx}, J_{2yy}, J_{2zz}$	Inertia Moment of Link 2 Computed with Respect to its Center of Mass;	0.012196 kg·m^2 0.100620 kg·m^2 0.095789 kg·m^2
g	Gravitational Acceleration	9.80665 m/s^2

In order to demonstrate the robustness of the control scheme proposed in this paper, modeling error, frictional disturbance, and external disturbance are introduced in the

robotic manipulator system. In this paper, 80% of the dynamic parameters of the robotic manipulator system are considered nominal, and 20% of the system dynamic parameters are considered modeling errors.

$$\begin{gathered} M_0(q) = 0.8M(q), \Delta M(q) = 0.2M(q) \\ C_0(q,\dot{q}) = 0.8C(q,\dot{q}), \Delta C(q,\dot{q}) = 0.2C(q,\dot{q}) \\ G_0(q) = 0.8G(q), \Delta G(q) = 0.2G(q) \end{gathered} \tag{43}$$

Let the external disturbances $\begin{bmatrix} \tau_{d1} \\ \tau_{d2} \end{bmatrix} = \begin{bmatrix} \tau_{1d1} \\ \tau_{2d1} \end{bmatrix} + \begin{bmatrix} \tau_{1d2} \\ \tau_{2d2} \end{bmatrix} + \begin{bmatrix} \tau_{1d3} \\ \tau_{2d3} \end{bmatrix}$ be time-varying, where $\begin{bmatrix} \tau_{1d1} \\ \tau_{2d1} \end{bmatrix}$ is a small magnitude time-varying disturbance and $\begin{bmatrix} \tau_{1d2} \\ \tau_{2d2} \end{bmatrix}$ is a joint viscous friction and coulomb friction. In order to verify the effectiveness of the proposed adaptive algorithm, an unknown large magnitude time-varying disturbance is introduced at the 10th second.

$$\begin{aligned} \begin{bmatrix} \tau_{d1} \\ \tau_{d2} \end{bmatrix} &= \begin{bmatrix} \tau_{1d1} \\ \tau_{2d1} \end{bmatrix} + \begin{bmatrix} \tau_{1d2} \\ \tau_{2d2} \end{bmatrix} + \begin{bmatrix} \tau_{1d3} \\ \tau_{2d3} \end{bmatrix} \\ &= \begin{bmatrix} 5 \times \sin(t) \\ 5 \times \sin(2t) \end{bmatrix} + \begin{bmatrix} 0.5\sin(\dot{q}) + 0.5\dot{q} \\ 0.5\sin(\dot{q}) + 0.5\dot{q} \end{bmatrix} + \begin{bmatrix} 25\cos(2 \times (\mathrm{t} - 10)) \\ 25\cos(3 \times (\mathrm{t} - 10)) \end{bmatrix} \end{aligned} \tag{44}$$

Next, to perform simulations to prove the effectiveness of the control scheme proposed in this paper, two control algorithms are disassembled based on the controller proposed: one is perturbation observer-based non-singular terminal sliding mode control (NDONTSM), and the other is perturbation observer-based adaptive non-singular terminal sliding mode control (NDOANTSM). The two types of PID and NDOPID are reintroduced. Control algorithms are compared and analyzed.

1. PID: This is a proportional–integral differential controller with the following control rates:

$$\tau = k_p e + k_i \int_0^t e + k_d \dot{e} \tag{45}$$

For the PID controller, k_p, k_i, k_d represent the coefficients of proportional, integral and differential, respectively. The parameters of k_p, k_i, k_d are selected mainly by experience and debugging, and the selection principle is to reduce the oscillation of the initial link of position tracking as much as possible and ensure the accuracy of trajectory tracking.

2. NDOPID: This is a proportional–integral differential controller that introduces a nonlinear disturbance observer to estimate the external disturbances, the control rate is as follows:

$$\tau = k_p e + k_i \int_0^t e + k_d \dot{e} - \hat{F}_d \tag{46}$$

For the NDOPID controller, the same coefficients of k_p, k_i, k_d are selected as for the PID. X^{-1} is an invertible matrix used to compute the observer gain matrix and auxiliary variables, which are obtained by solving LMI, and the same values are taken in all the controllers in order to ensure the fairness of the controller comparison.

Considering the limitation of the output torque of the actual robotic arm joints, the output torque τ of both PID and NDOPID controllers is limited at $-50\ \mathrm{N \cdot m} < \tau < 50\ \mathrm{N \cdot m}$. The following methods can be adopted to manage input saturation in the controller. Method 1 is for cases in which the input saturation boundary is known. First, the compensation of control saturation can be achieved by designing a stable adaptive auxiliary system with dynamic amplification of input saturation error. The second method is for cases in which the input saturation boundary is unknown; in this method, we can set the error of the

theoretical input saturation boundary as δ, approximate δ by designing an RBF network, and feedback the approximation value $\hat{\delta}$ to the controller for compensation.

3. NDONTSM: This is an NTSM controller based on a disturbance observer without an s term robust adaptive law anda $sign()$ term switching adaptive law; it has the following control laws:

$$\begin{aligned} \tau = & \quad \tau_{\text{eq}} + \tau_{\text{sw}} - \hat{F}_d \\ = & \quad M_0(q)\ddot{q}_d + C_0(q,\dot{q})\dot{q} + G_0(q) - \beta\frac{r}{p}|\varepsilon_2|^{2-\frac{p}{r}} sign(\varepsilon_2) \\ & -M_0(\mathrm{k_1 s} + \mathrm{k_2 sig}n(\mathrm{s})) - \hat{F}_d \end{aligned} \tag{47}$$

For the NDONTSM controller, β, p, r are the parameters of the sliding mode surface, $\beta > 0, p, r$ are positive integers and $1 < p/r < 2$. For the three parameters $p = 5, r = 3$, in order to ensure the non-singularity of the sliding mode surface, $\beta = 20$, and the same value is set in the NDOANTSM and PNDOANTSM controllers to ensure fairness in the controller comparison.

4. NDOANTSM: This is an ANTSM controller based on a disturbance observer, excluding the s term robust adaptive law, with the following control law:

$$\begin{aligned} \tau = & \quad \tau_{\text{eq}} + \tau_{\text{sw}} - \hat{F}_d \\ = & \quad M_0(q)\ddot{q}_d + C_0(q,\dot{q})\dot{q} + G_0(q) - \beta\frac{r}{p}|\varepsilon_2|^{2-\frac{p}{r}} sign(\varepsilon_2) \\ & -M_0(\mathrm{k_1 s} + (\hat{b}_0 + \hat{b}_1 \parallel q \parallel + \hat{b}_2 \parallel \dot{q} \parallel^2)\mathrm{sig}n(\mathrm{s})) - \hat{F}_d \end{aligned} \tag{48}$$

$$\begin{aligned} \dot{\hat{b}}_0 &= \begin{cases} \lambda_0 \parallel s \parallel |\varepsilon_2|^{\frac{p}{r}-1}, \text{if} \parallel s \parallel \geq \xi \\ 0, \text{if} \parallel s \parallel < \xi \end{cases} \\ \dot{\hat{b}}_1 &= \begin{cases} \lambda_1 \parallel s \parallel\parallel q \parallel |\varepsilon_2|^{\frac{p}{r}-1}, \text{if} \parallel s \parallel \geq \xi \\ 0, \text{if} \parallel s \parallel < \xi \end{cases} \\ \dot{\hat{b}}_2 &= \begin{cases} \lambda_2 \parallel s \parallel\parallel q \parallel^2 |\varepsilon_2|^{\frac{p}{r}-1}, \text{if} \parallel s \parallel \geq \xi \\ 0, \text{if} \parallel s \parallel < \xi \end{cases} \end{aligned} \tag{49}$$

For NDOANTSM controllers, $\beta = 20$, $p = 5$, $r = 3$, $\mathrm{k_1} = 1500$, $X^{-1} = \begin{bmatrix} 3.5249 & 0 \\ 0 & 2.8547 \end{bmatrix}$ are consistent with those in NDONTSM controllers to ensure fairness. $\lambda_i = 60$, $\xi = 0.008$, λ_i is the gain coefficient of the switching gain adaptive rate, and the value of λ_i determines how fast or slow the switching gain adaptive rate is updated; for time-varying perturbations, a larger value can be chosen to facilitate the rapid arrival at the upper bounds of the perturbation. ξ is the trigger boundary used to set the switching adaptive rate; because of measurement noise and switching delays, $\|s\|$ cannot always be exactly zero, so the adaptive parameter may increase slowly and indefinitely. This drawback can be overcome by using the deadband technique, where ξ is usually chosen to be a small positive number.

5. PNDOANTSM: This is the adaptive non-singular terminal sliding mode controller based on a disturbance observer proposed in this paper; it has the following control law:

$$\begin{aligned} \tau = & \quad \tau_{\text{eq}} + \tau_{\text{asw}} - \hat{F}_d \\ = & \quad M_0\ddot{q}_d + C_0\dot{q} + G_0 - \beta\frac{r}{p}|\varepsilon_2|^{2-\frac{p}{r}} sign(\varepsilon_2) \\ & -M_0(\mathrm{k_0}(1+\hat{a}_0)s + (\hat{b}_0 + \hat{b}_1 \parallel q \parallel + \hat{b}_2 \parallel \dot{q} \parallel^2) sign(s)) - \hat{F}_d \end{aligned} \tag{50}$$

$$\begin{cases} \dot{\hat{a}}_0 = \begin{cases} H_0 \parallel s \parallel^2 |\varepsilon_2|^{\frac{p}{r}-1}, \text{if} \parallel s \parallel \geq \xi \cap \parallel \hat{F}_d \parallel \geq \gamma \\ 0, \text{if} \parallel s \parallel < \xi \end{cases} \\ \dot{\hat{b}}_0 = \begin{cases} \lambda_0 \parallel s \parallel |\varepsilon_2|^{\frac{p}{r}-1}, \text{if} \parallel s \parallel \geq \xi \\ 0, \text{if} \parallel s \parallel < \xi \end{cases} \\ \dot{\hat{b}}_1 = \begin{cases} \lambda_1 \parallel s \parallel \parallel q \parallel |\varepsilon_2|^{\frac{p}{r}-1}, \text{if} \parallel s \parallel \geq \xi \\ 0, \text{if} \parallel s \parallel < \xi \end{cases} \\ \dot{\hat{b}}_2 = \begin{cases} \lambda_2 \parallel s \parallel \parallel q \parallel^2 |\varepsilon_2|^{\frac{p}{r}-1}, \text{if} \parallel s \parallel \geq \xi \\ 0, \text{if} \parallel s \parallel < \xi \end{cases} \end{cases} \tag{51}$$

For PNDOANTSM controllers, $\beta = 20$, $p = 5$, $r = 3$, $\mathrm{k}_0 = 1500$, $\lambda_i = 60$, $\xi = 0.008$, $X^{-1} = [3.5249 \quad 0; \quad 0 \quad 2.8547]$. The parameter settings are the same as those for the NDOANTSM controller. This controller adds a new robust adaptive law relative to that of the NDOANTSM controller, $H_0 = 800$, $\gamma = 5$, where H_0 is the gain coefficient of the robust adaptive rate; when the system encounters a large perturbation in an instant, the state variables are out of the sliding mode surface. Therefore, the coefficients of the s term robust adaptive rate need to be adjusted quickly so that the state variables can converge to the sliding mode surface again, and H_0 can be chosen as a large positive number. γ is the trigger boundary of the robust adaptive rate, and in this paper, we set it to be judged as a larger perturbation when the maximum perturbation observed by the observer exceeds 5 N · m.

The parameter settings for the five control laws above are shown in Table 2.

Table 2. Parameter settings in the control law.

Control Law	Parameter Settings
PID	$k_p = \begin{bmatrix} 400 & 0 \\ 0 & 500 \end{bmatrix}, k_i = \begin{bmatrix} 150 & 0 \\ 0 & 150 \end{bmatrix}, k_d = \begin{bmatrix} 20 & 0 \\ 0 & 30 \end{bmatrix}$
NDOPID	$k_p = \begin{bmatrix} 400 & 0 \\ 0 & 500 \end{bmatrix}, k_i = \begin{bmatrix} 150 & 0 \\ 0 & 150 \end{bmatrix}, k_d = \begin{bmatrix} 20 & 0 \\ 0 & 30 \end{bmatrix}$
NDONTSM	$X^{-1} = \begin{bmatrix} 3.5249 & 0 \\ 0 & 2.8547 \end{bmatrix}$
	$\beta = 20, p = 5, r = 3, \mathrm{k}_1 = 1500, \mathrm{k}_2 = 2,$
	$X^{-1} = \begin{bmatrix} 3.5249 & 0 \\ 0 & 2.8547 \end{bmatrix}$
NDOANTSM	$\beta = 20, p = 5, r = 3, \mathrm{k}_1 = 1500, \lambda_i = 60, \xi = 0.008,$
	$X^{-1} = \begin{bmatrix} 3.5249 & 0 \\ 0 & 2.8547 \end{bmatrix}$
PNDOANTSM	$\beta = 20, p = 5, r = 3, \mathrm{k}_0 = 1500,$
	$\lambda_i = 60, \xi = 0.008, H_0 = 800, \gamma = 5,$
	$X^{-1} = \begin{bmatrix} 3.5249 & 0 \\ 0 & 2.8547 \end{bmatrix}$

The simulation results of the above five algorithms are shown in Figures 5–11. The position tracking of robotic manipulator joints 1 and 2 is presented in Figure 5. Position tracking errors of robotic manipulator joints 1 and 2 are presented in Figures 6 and 7. The control input moments of robotic manipulator joints 1 and 2 are presented in Figure 8. The PNDOANTSM algorithm proposed in this paper and the adaptive parameter variations in the NDOANTSM algorithm are presented in Figure 9. The disturbances to robotic manipulator joints 1 and 2 observed by the nonlinear disturbance observer used in this paper are presented in Figure 10, while the disturbance observation error is presented in Figure 11.

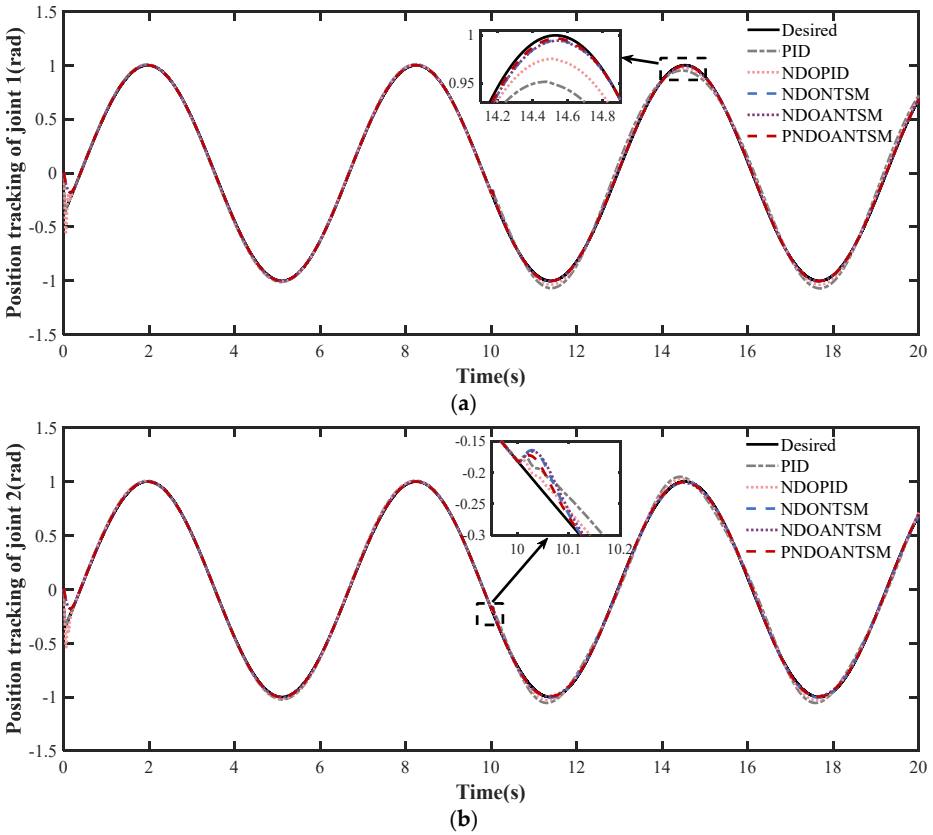


Figure 5. Position tracking performance of joint 1 and joint 2. (**a**) Position tracking performance of joint 1; (**b**) position tracking performance of joint 2.

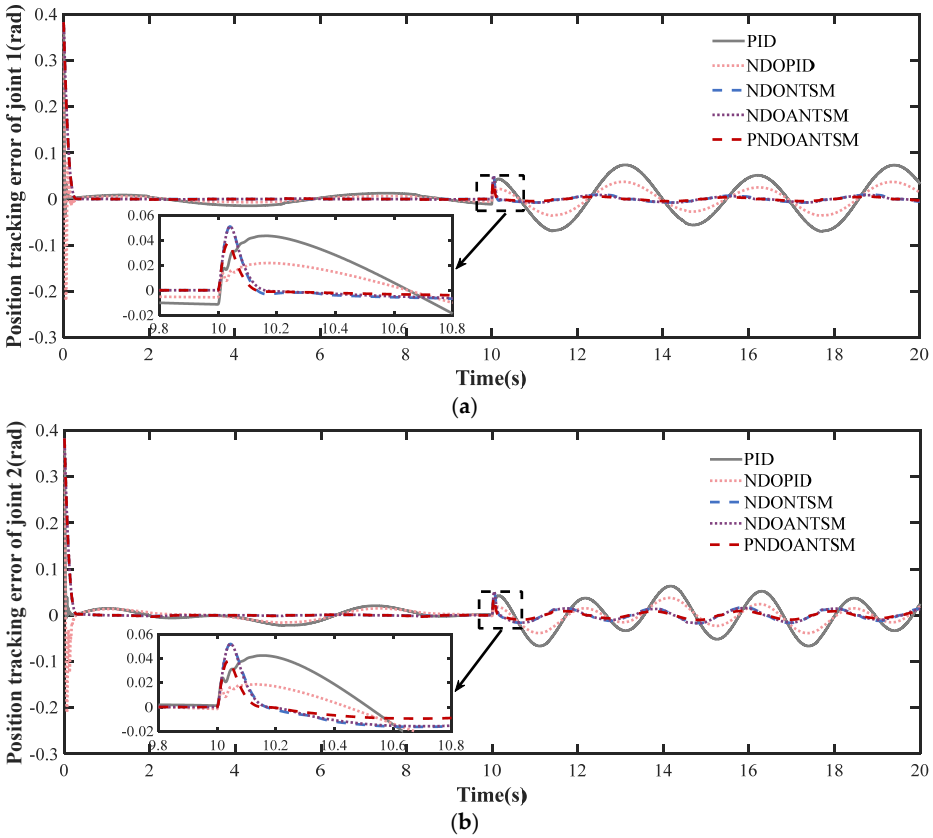


Figure 6. Position tracking errors of joint 1 and joint 2. (**a**) Position tracking errors of joint 1; (**b**) position tracking errors of joint 2.

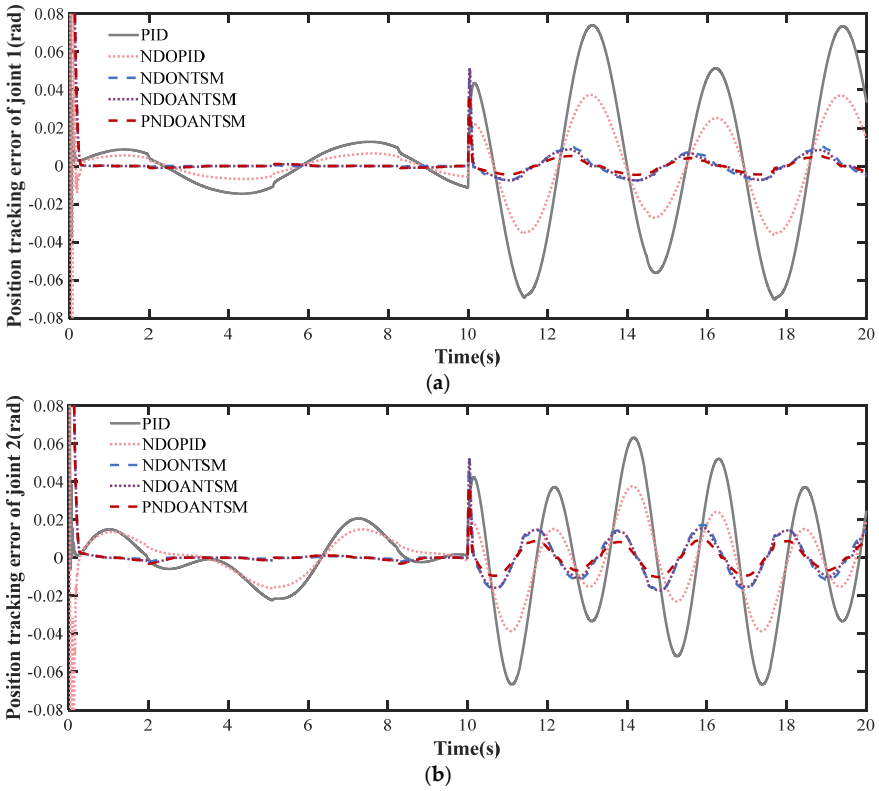


Figure 7. Localized enlargement of position tracking error for joint 1 and joint 2. (**a**) Localized enlargement of position tracking error for joint 1; (**b**) localized enlargement of position tracking error for joint 2.

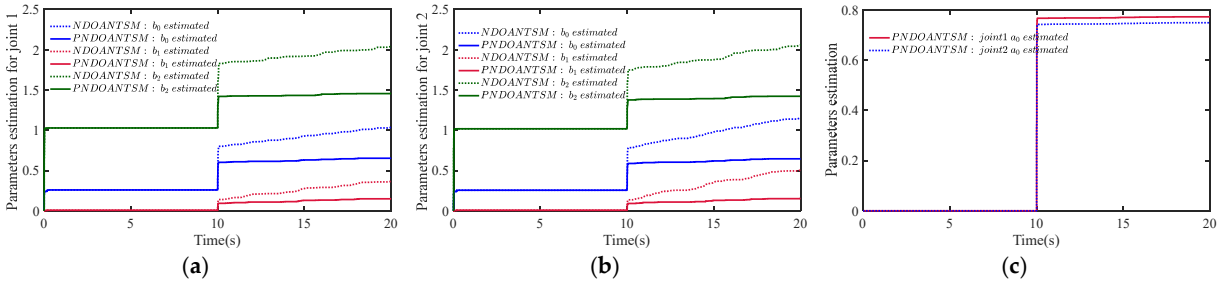


Figure 8. Adaptation of parameter estimation. (**a**) Variation in values of adaptive parameters $\hat{b}_0, \hat{b}_1, \hat{b}_2$ for robotic manipulator joint 1 in the PNDOANTSM algorithm and the NDOANTSM algorithm; (**b**) variation in values of adaptive parameters $\hat{b}_0, \hat{b}_1, \hat{b}_2$ for robotic manipulator joint 2 in the PNDOANTSM algorithm and the NDOANTSM algorithm; (**c**) variation in the values of the adaptive parameter $\hat{a}_0$ for robotic manipulator joints 1 and 2 in the PNDOANTSM algorithm.

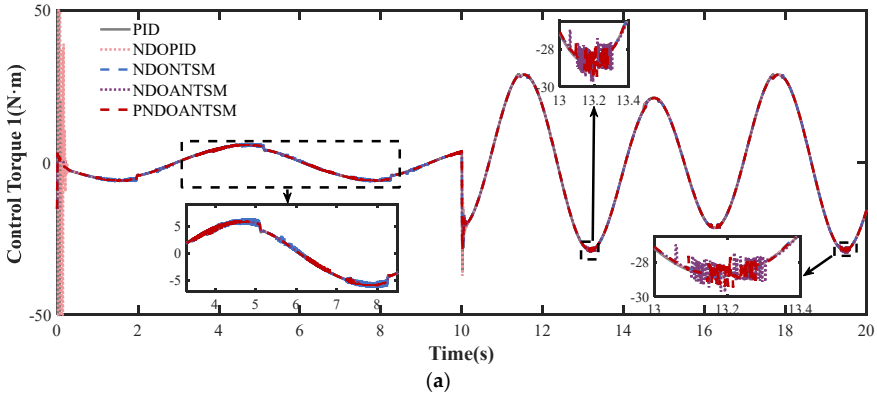


Figure 9. *Cont*.

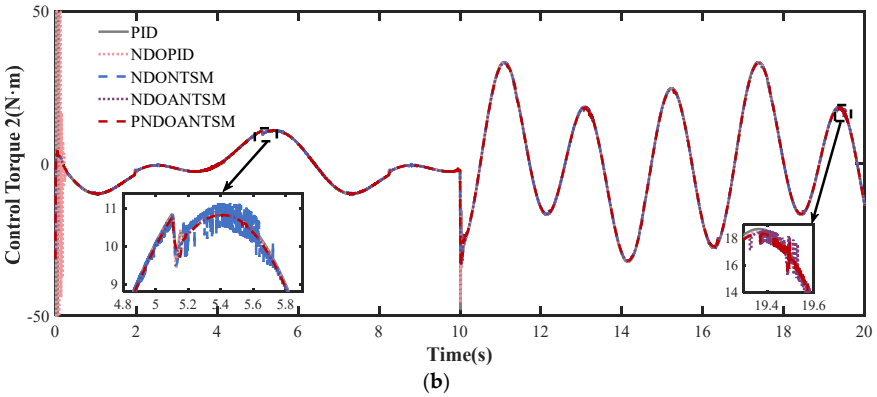


Figure 9. Control input torques of joint 1 and joint 2. (**a**) Control input torque of joint 1; (**b**) control input torque of joint 2.

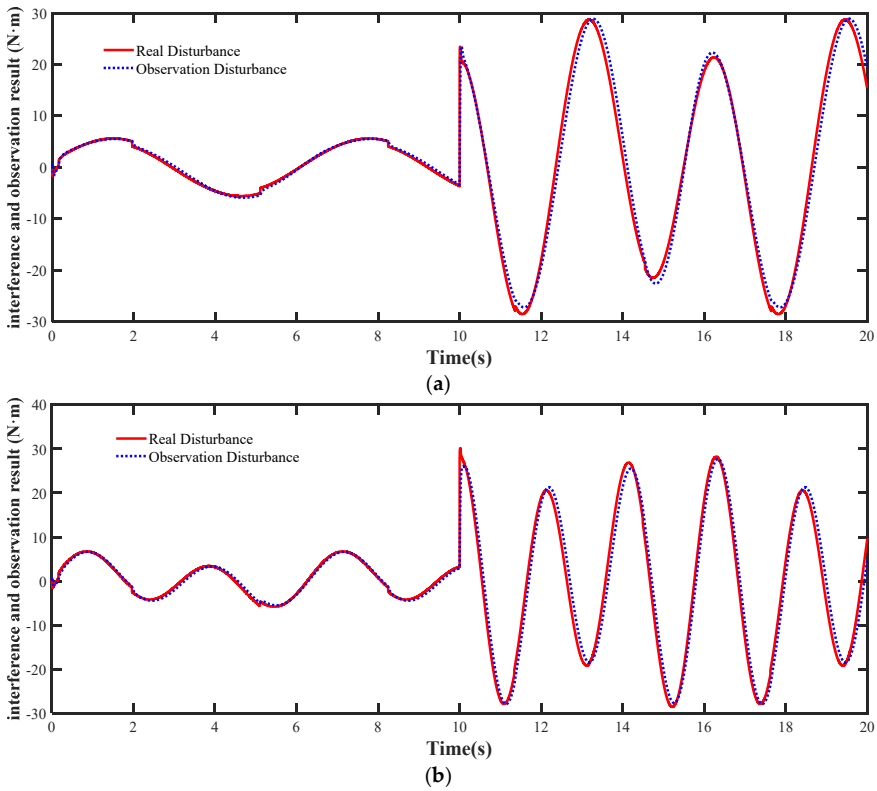


Figure 10. Interference and observation results of joint 1 and joint 2. (**a**) Interference and observation result of joint 1; (**b**) interference and observation result of joint 2.

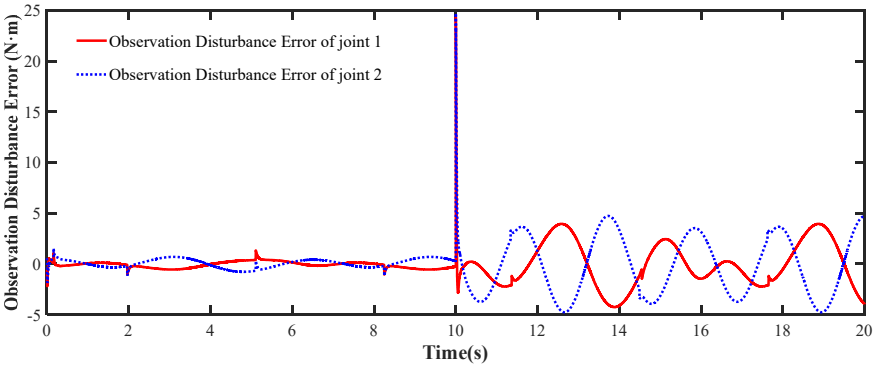


Figure 11. Observation disturbance error of joint 1 and joint 2.

To further compare the dynamic characteristics of the five control algorithms, this paper takes the mean steady-state error (MSE) of the joint angles, the integral of the absolute value of the error (IAE), given by IAE $= \int_0^{t_f} \mid e(t) \mid dt$, the integral of the time multiplied by the absolute value of the error (ITAE), given by ITAE $= \int_0^{t_f} t \cdot \mid e(t) \mid dt$, which t_f denotes the total running time. The specific performance metrics are shown in Tables 2 and 3, which are used to evaluate the performance of the controller.

Table 3. Mean steady-state error evaluation indexes.

Controllers	Joints	Mean Steady-State Error (rad)	
		1–10 (s)	11–20 (s)
PNDOANTSM	Joint 1	3.0221×10^{-4}	0.0026
	Joint 2	6.1377×10^{-4}	0.0052
NDOANTSM	Joint 1	3.0221×10^{-4}	0.0041
	Joint 2	6.1377×10^{-4}	0.0084
NDONTSM	Joint 1	2.6879×10^{-5}	0.0047
	Joint 2	2.9483×10^{-4}	0.0091
NDOPID	Joint 1	0.0042	0.0218
	Joint 2	0.0073	0.0163
PID	Joint 1	0.0081	0.0434
	Joint 2	0.0087	0.0314

Analyzing Figure 5 shows that all five algorithms can track a specific trajectory within a certain error range. By analyzing the error curves in Figures 6 and 7, it can be seen that in the 0–10 s phase, PID and NDOPID have large oscillations in the position error curves before the steady state, and NDONTSM, NDOANTSM, and PNDOANTSM can enter the steady state at a faster speed and with no error oscillations.

The tracking errors of robotic manipulator joints 1 and 2 can be seen by analyzing the local zoomed-in graphs in Figure 6. At the 10th second, the robotic manipulator suffers from unknown external interference, and the maximum position tracking errors of joints 1 and 2 of the robotic manipulator proposed in this paper are 0.0378 rad and 0.0377 rad after the impact of the large interference. The maximum position tracking errors of the robotic manipulator joints applying the NDOANTSM and NDONTSM algorithms are the same. The maximum position tracking errors of joint 1 are both 0.0511 rad, and the maximum position tracking errors of joint 2 are both 0.0518 rad.

By analyzing the position tracking error local amplification in Figure 7, it can be observed that the steady-state error of the PNDOANTSM algorithm is smaller than that of the other four algorithms after it enters the steady state in 10–20 s. The 11–20 s interval is selected to calculate the average steady-state error, as shown in Table 3.

The average steady-state error of the PNDOANTSM algorithm for joints 1 and 2 is reduced by 36.58% and 38.40% compared to that of the NDOANTSM algorithm, 44.68% and 42.86% compared to that of the NDONTSM algorithm, 88.07% and 68.10% compared to that of the NDOPID algorithm, and 94.01% and 83.44% compared to that of the PID algorithm.

Combined with the performance metrics analysis of Table 4, the IAE metrics for joints 1 and 2 of the PNDOANTSM algorithm are optimal in the 0–20 s interval. The IAE metrics of joints 1 and 2 of the PNDOANTSM algorithm compared to those of the NDOANTSM algorithm are reduced by 20.10% and 26.35%. The IAE metrics of joints 1 and 2 of the PNDOANTSM algorithm with the NDONTSM algorithm are reduced by 23.39% and 28.70%. The IAE metrics of the PNDOANTSM algorithm with the NDONTSM algorithm are reduced by 76.43% and 63.66%. The IAE metrics of the PNDOANTSM algorithm are reduced by 87.41%, 77.06% compared with those of the PID algorithm. According to Table 4, the ITAE metrics of joints 1 and 2 in the PNDOANTSM algorithm are also the lowest among those of the five algorithms.

Table 4. Comparison of IAE and ITAE performance parameters for five algorithms.

Controllers	Joints	IAE (rad)			ITAE (rad·s)
		0–10 (s)	10–20 (s)	0–20 (s)	
PNDOANTSM	Joint 1	0.0351	0.0281	0.0632	0.4249
	Joint 2	0.0387	0.0552	0.0939	0.8456
NDOANTSM	Joint 1	0.0351	0.0440	0.0791	0.6539
	Joint 2	0.0387	0.0888	0.1275	1.3353
NDONTSM	Joint 1	0.0325	0.0500	0.0825	0.7367
	Joint 2	0.0357	0.0960	0.1317	1.4380
NDOPID	Joint 1	0.0589	0.2092	0.2681	3.3844
	Joint 2	0.0943	0.1641	0.2584	2.7757
PID	Joint 1	0.0859	0.4159	0.5018	6.7250
	Joint 2	0.0944	0.3147	0.4093	5.0909

Next, the performance metrics of the five algorithms in Table 4 are analyzed from other perspectives to illustrate the effectiveness of the algorithms proposed in this paper. These include the nonlinear disturbance observer, NTSM, the $sign()$ term switching adaptive algorithm, and the s term robust adaptive algorithm. Introducing a nonlinear observer for PID reduces the IAE metrics for robotic manipulator joints 1 and 2 by 46.57% and 36.87% compared with those of the PID without the nonlinear observer. This indicates the effectiveness of the nonlinear observer. The IAE metrics of the NDONTSM algorithm for robotic manipulator joints 1 and 2 are reduced by 68.49% and 49.03% compared to that of the NDOPID algorithm, which indicates that the NTSM algorithm's tracking performance is better than that of the PID algorithm under large disturbances. The IAE metrics of the robotic manipulator joints 1 and 2 NDOANTSM algorithm are reduced by 12.85% and 3.19% compared with those of the NDONTSM algorithm. This shows the effectiveness of introducing the $sign()$ term in the switching adaptive algorithm. Its adaptive parameters $\hat{b}_0, \hat{b}_1, \hat{b}_2$ are varied, as shown in Figure 8a,b. The IAE metrics of robotic manipulator joints 1 and 2 in the PNDOANTSM algorithm is reduced by 20.10% and 26.35% compared those of to the NDOANTSM algorithm. This shows the effectiveness of introducing the s term switching adaptive algorithm. Its adaptive parameter $\hat{a}_0$ variation is shown in Figure 8c.

At the 0–10 s stage, the observer observes a disturbance of less than 5 N · m, and the adaptive parameter $\hat{a}_0$ is 0. At the 10th second, the robotic manipulator is subjected to a large unknown disturbance. The observer observes a disturbance greater than 5 N · m, and the sliding mode surface norm $\| s \|$ is greater than 0.008. The adaptive parameter $\hat{a}_0$ is updated. Meanwhile, the $sign()$ term switching adaptive law parameter change of the NDOANTSM algorithm without the s term robust adaptive law introduced into it shows a trend of great increase after being subjected to a large disturbance shock for 10–20 s, as shown in Figure 8a,b. Because this disturbance is time-varying, the adaptive parameter is updated only when the value of the disturbance is large, when the sliding mode surface norm $\| s \|$ is greater than 0.008. Thus, the reason for producing adaptive parameters $\hat{b}_0$, $\hat{b}_1$ and $\hat{b}_2$ that have an exponentially increasing trend is that it is impossible to estimate the unknown time-varying large disturbances in a short period.

Considering the actual robotic manipulator torque input is limited, the control torque input of the robotic manipulator in the PID and NDOPID algorithms is limited to [−50 N · m, 50 N · m], and analyzing Figure 9 shows that in at the 0–10 s stage, i.e., the initial stage of the PID and NDOPID algorithms, the inputs will show a large torque oscillation. NDONTSM experiences jitter, which is because the NDONTSM algorithm does not include the $sign()$ term switching adaptive law, therefore failing to accurately estimate the interference in the upper bound. Combined with Table 2, the IAE error of the NDONTSM algorithm is smaller than that of the NDOANTSM and PNDOANTSM algorithms for 0–10 s. For time-varying disturbances, to ensure a smaller steady-state error, the gain in the fixed $sign()$ term is slightly larger than the maximum value in the time-varying disturbances

needed to cover the disturbance uncertainty, which results in the jittering of the input torque when the time-varying disturbances are small.

Since the NDOANTSM and PNDOANTSM algorithms introduce the $sign()$ adaptive term to estimate the upper bound of the disturbance and adjust the gain of the signed term according to the adaptive rate, the input torque jitter is smaller at the 0–10 s stage, as shown in Figure 9. Analyzing the locally enlarged block diagram in Figure 9, the PNDOANTSM algorithm introduces the robust adaptive law of the s term at the stage of large unknown disturbances in 10–20 s, and the input torque jitter amplitude is smaller compared with that of the NDOANTSM algorithm.

Analyzing Figure 10 shows that the nonlinear interference observer is included in the PNDOANTSM algorithm proposed in this paper. It can be seen that the disturbances were suffered by robotic arm joints 1 and 2 at the same time, and the observed disturbance error is shown in Figure 11.

5. Conclusions

This paper investigates trajectory tracking control algorithms for robotic manipulators. The main innovations of this work are as follows:

(1) In the case of system modeling uncertainty and large external unknown time-varying disturbances, in this paper, a novel adaptive non-singular terminal sliding mode control method based on a nonlinear disturbance observer is proposed, and system stability and finite time convergence are proven by the Lyapunov method.

(2) The controller employs an improved nonlinear disturbance observer, which performs feed-forward compensation by observing the robotic manipulator modeling error and the external unknown time-varying disturbances to which each joint is subjected. Thus, the switching gain only needs to cover the perturbation observation error and not the total perturbation, avoiding the jitter caused by the too-large gain coefficients of the switching term and improving the system's robustness.

(3) Eschewing the need to know the system uncertainty and perturbation bounds, the set-total perturbation adaptive law, i.e., the $sign()$ switching term gain adaptive law, is devised to estimate the upper bound of the observed perturbation error of the system without the need for an a priori upper bound on the system's uncertainty and external disturbances.

(4) The s-term robust adaptive law is triggered by introducing the observation disturbance and the magnitude of the sliding mode surface term norm error. The s-term coefficients are adapted simultaneously when subjected to unknown time-varying disturbances to improve the system's robustness.

(5) Finally, the designed PNDOANTSM controller is applied to the trajectory tracking control simulation of the two-link robotic space manipulator. It has higher trajectory tracking accuracy and stability compared with PID, NDOPID, NDONTSM, and NDOANTSM, and the controller embodies strong robustness in the case of large unknown time-varying interference from the outside world.

The research in this paper provides a basis for the trajectory tracking control of robotic manipulators with system modeling uncertainties and the presence of large disturbances. In addition, experiments will be conducted in the future to verify the effect of the trajectory tracking control algorithm, which is expected to be applied in the high-precision trajectory tracking tasks carried out by robotic arm equipment. The control algorithm proposed in this paper has some potential difficulties when deployed in practice: it involves real-time disturbance observation and adaptive parameter tuning, which may increase the system's computational burden. The demand for computational resources may become a limiting factor when dealing with complex trajectory tracking. Furthermore, although the observer

can observe some external disturbances, there is still an observation error. The system's observation results may be affected by extreme external high-frequency disturbances.

Author Contributions: S.Y. and Z.S. contributed to the conceptualization of this paper. S.Y. designed the controller and wrote the paper; H.Y. analyzed the data; G.X. and Y.L. reviewed and edited the paper; Y.L. and G.X. contributed to funding acquisition, supervision, and project administration. All authors have read and agreed to the published version of the manuscript.

Funding: The research was supported by the Key Research and Development Plan of Shandong Province—Major Science and Technology Innovation Project (No. 2022CXGC010608), the National Key Research and Development Program of China (No. 2023YFC2810100), the National Natural Science Foundation of China (No. 42188102), and the Open Fund of State Key Laboratory of Mechanical Transmission for Advanced Equipment (SKLMT-KFKT-202214), to which the authors are grateful.

Data Availability Statement: The original contributions presented in this study are included in the article. Further inquiries can be directed to the corresponding author(s).

Acknowledgments: Here, I would like to thank Yanjun Liu and Gang Xue for their technical support during the research.

Conflicts of Interest: There are no conflicts of interest regarding the research for this thesis.

References

1. Duan, J.G.; Zhang, H.Z.; Zhang, Q.L.; Qin, J.Y. Research on Neural Network Terminal Sliding Mode Control of Robotic Arms Based on Novel Reaching Law and Improved Salp Swarm Algorithm. *Actuators* **2023**, *12*, 464. [CrossRef]
2. Arefi, M.M.; Vafamand, N.; Homayoun, B.; Davoodi, M. Command Filtered Backstepping Control of Constrained Flexible Joint Robotic Manipulator. *IET Contr. Theory Appl.* **2023**, *17*, 2506–2518. [CrossRef]
3. Ai, W.X.; Pan, X.N.; Jiang, Y.; Wang, H.G. Neural Admittance Control Based on Motion Intention Estimation and Force Feedforward Compensation for Human-Robot Collaboration. *Int. J. Intell. Robot.* **2024**, *8*, 560–573. [CrossRef]
4. Yang, S.C.; Xie, H.H.; Chen, F.; Zhang, J.B.; Feng, S.; Liu, J. Research on Manipulator Trajectory Tracking Based on Adaptive Fuzzy Sliding Mode Control. In Proceedings of the 2020 Chinese Automation Congress (CAC), Shanghai, China, 6–8 November 2020.
5. Zhao, H.Y.; Tao, B.; Ma, R.Y.; Chen, B.J. Manipulator Trajectory Tracking Based on Adaptive Fuzzy Sliding Mode Control. *Concurr. Comput. Pract. Exp.* **2023**, *35*, e7620. [CrossRef]
6. Chen, J.Q.; Zhang, H.Y.; Tang, Q.S.; Zhang, H.D. Adaptive Fuzzy Sliding Mode Control of the Manipulator Based on an Improved Super-Twisting Algorithm. *Proc. Inst. Mech. Eng. Part C J. Mech. Eng. Sci.* **2024**, *238*, 4294–4306. [CrossRef]
7. Tang, J.; Ouyang, P.R.; Yue, W.H.; Kang, H.M. Nonlinear Pd Sliding Mode Control for Robotic Manipulator. In Proceedings of the IEEE International Conference on Advanced Intelligent Mechatronics (AIM), Munich, Germany, 3–7 July 2017.
8. Xiong, R.; Li, L.J.; Zhang, C.X.; Ma, K.; Yi, X.S.; Zeng, H.S. Path Tracking of a Four-Wheel Independently Driven Skid Steer Robotic Vehicle through a Cascaded Ntsm-Pid Control Method. *IEEE Trans. Instrum. Meas.* **2022**, *71*, 11. [CrossRef]
9. Hu, Y.S.; Yan, H.C.; Zhang, H.; Wang, M.; Zeng, L. Robust Adaptive Fixed-Time Sliding-Mode Control for Uncertain Robotic Systems with Input Saturation. *IEEE Trans. Cybern.* **2023**, *53*, 2636–2646. [CrossRef]
10. Zhang, Y.Y.; Yang, X.H.; Wei, P.; Liu, P.X. Fractional-Order Adaptive Non-Singular Fast Terminal Sliding Mode Control with Time Delay Estimation for Robotic Manipulators. *IET Control. Theory Appl.* **2020**, *14*, 2556–2565. [CrossRef]
11. Cao, S.J.; Sun, L.; Jiang, J.J.; Zuo, Z.Y. Reinforcement Learning-Based Fixed-Time Trajectory Tracking Control for Uncertain Robotic Manipulators with Input Saturation. *IEEE Trans. Neural Netw. Learn. Syst.* **2023**, *34*, 4584–4595. [CrossRef] [PubMed]
12. Zhai, A.B.; Wang, J.; Zhang, H.Y.; Lu, G.D.; Li, H.W. Adaptive Robust Synchronized Control for Cooperative Robotic Manipulators with Uncertain Base Coordinate System. *ISA Trans.* **2022**, *126*, 134–143. [CrossRef] [PubMed]
13. Zhang, Y.; Lei, Y.Q.; Zhang, T.C.; Song, R.; Li, Y.B.; Du, F.X. Robust Command-Filtered Control with Prescribed Performance for Flexible-Joint Robots. *IEEE Trans. Instrum. Meas.* **2023**, *72*, 13. [CrossRef]
14. Wang, Y.; Liu, Y.T.; Xu, F. Adaptive Iterative Learning Control of Soft Robot for Beating Heart Tracking. *Robot. Intell. Autom.* **2024**, *44*, 488–497. [CrossRef]
15. Yan, J.K.; Jin, L.; Hu, B. Data-Driven Model Predictive Control for Redundant Manipulators with Unknown Model. *IEEE Trans. Cybern.* **2024**, *54*, 5901–5911. [CrossRef] [PubMed]
16. Busoniu, L.; de Bruin, T.; Tolic, D.; Kober, J.; Palunko, I. Reinforcement Learning for Control: Performance, Stability, and Deep Approximators. *Annu. Rev. Control* **2018**, *46*, 8–28. [CrossRef]

17. Yang, L.; Yang, J.Y. Nonsingular Fast Terminal Sliding-Mode Control for Nonlinear Dynamical Systems. *Int. J. Robust Nonlinear Control* **2011**, *21*, 1865–1879. [CrossRef]
18. Li, P.; Ma, J.J.; Zheng, Z.Q.; Geng, L.N. Fast Nonsingular Integral Terminal Sliding Mode Control for Nonlinear Dynamical Systems. In Proceedings of the 53rd IEEE Annual Conference on Decision and Control (CDC), Los Angeles, CA, USA, 15–17 December 2014.
19. Zhang, L.Y.; Su, Y.X.; Wang, Z. A Simple Non-Singular Terminal Sliding Mode Control for Uncertain Robot Manipulators. *Proc. Inst. Mech. Eng. Part I J. Syst. Control. Eng.* **2019**, *233*, 666–676. [CrossRef]
20. Chen, W.H.; Ballance, D.J.; Gawthrop, P.J.; O'Reilly, J. A Nonlinear Disturbance Observer for Robotic Manipulators. *IEEE Trans. Ind. Electron.* **2000**, *47*, 932–938. [CrossRef]
21. Mohammadi, A.; Tavakoli, M.; Marquez, H.J.; Hashemzadeh, F. Nonlinear Disturbance Observer Design for Robotic Manipulators. *Control Eng. Pract.* **2013**, *21*, 253–267. [CrossRef]
22. Yang, J.; Li, S.H.; Yu, X.H. Sliding-Mode Control for Systems with Mismatched Uncertainties Via a Disturbance Observer. *IEEE Trans. Ind. Electron.* **2013**, *60*, 160–169. [CrossRef]
23. Neila, M.B.R.; Tarak, D. Adaptive Terminal Sliding Mode Control for Rigid Robotic Manipulators. *Int. J. Autom. Comput.* **2011**, *8*, 215–220. [CrossRef]
24. Boukattaya, M.; Mezghani, N.; Damak, T. Adaptive Nonsingular Fast Terminal Sliding-Mode Control for the Tracking Problem of Uncertain Dynamical Systems. *ISA Trans.* **2018**, *77*, 1–19. [CrossRef]
25. Yi, S.C.; Zhai, J.Y. Adaptive Second-Order Fast Nonsingular Terminal Sliding Mode Control for Robotic Manipulators. *ISA Trans.* **2019**, *90*, 41–51. [CrossRef]
26. Yang, Q.Y.; Ma, X.F.; Wang, W.; Peng, D.L. Adaptive Non-Singular Fast Terminal Sliding Mode Trajectory Tracking Control for Robot Manipulators. *Electronics* **2022**, *11*, 3672. [CrossRef]
27. Susca, M.; Mihaly, V.; Morar, D.; Dobra, P. Sampling Rate Optimization and Execution Time Analysis for Two-Degrees-of-Freedom Control Systems. *Mathematics* **2022**, *10*, 3449. [CrossRef]
28. Morar, D.; Mihaly, V.; Susca, M.; Dobra, P. Cascade Control for Two-Axis Position Mechatronic Systems. *Fractal Fract.* **2023**, *7*, 122. [CrossRef]
29. Rojsiraphisal, T.; Mobayen, S.; Asad, J.H.; Vu, M.T.; Chang, A.; Puangmalai, J. Fast Terminal Sliding Control of Underactuated Robotic Systems Based on Disturbance Observer with Experimental Validation. *Mathematics* **2021**, *9*, 1935. [CrossRef]
30. Alattas, K.A.; Vu, M.T.; Mofid, O.; El-Sousy, F.F.M.; Alanazi, A.K.; Awrejcewicz, J.; Mobayen, S. Adaptive Nonsingular Terminal Sliding Mode Control for Performance Improvement of Perturbed Nonlinear Systems. *Mathematics* **2022**, *10*, 1064. [CrossRef]
31. Tan, J.; Zhang, K.; Li, B.; Wu, A.G. Event-Triggered Sliding Mode Control for Spacecraft Reorientation with Multiple Attitude Constraints. *IEEE Trans. Aerosp. Electron. Syst.* **2023**, *59*, 6031–6043. [CrossRef]
32. Lu, Y.T.; Tan, C.; Ge, W.Q.; Zhao, Y.J.; Wang, G. Adaptive Disturbance Observer-Based Improved Super-Twisting Sliding Mode Control for Electromagnetic Direct-Drive Pump. *Smart Mater. Struct.* **2023**, *32*, 017001. [CrossRef]
33. Sun, Y.H.; Peng, Z.A.; Hu, J.P.; Ghosh, B.K. Event-Triggered Critic Learning Impedance Control of Lower Limb Exoskeleton Robots in Interactive Environments. *Neurocomputing* **2024**, *564*, 126963. [CrossRef]
34. Mofid, O.; Amirkhani, S.; Din, S.U.; Mobayen, S.; Vu, M.T.; Assawinchaichote, W. Finite-Time Convergence of Perturbed Nonlinear Systems Using Adaptive Barrier-Function Nonsingular Sliding Mode Control with Experimental Validation. *J. Vib. Control* **2023**, *29*, 3326–3339. [CrossRef]
35. Dinh, T.X.; Thien, T.D.; Anh, T.H.V.; Ahn, K.K. Disturbance Observer Based Finite Time Trajectory Tracking Control for a 3 Dof Hydraulic Manipulator Including Actuator Dynamics. *IEEE Access* **2018**, *6*, 36798–36809. [CrossRef]
36. Man, Z.H.; O'Day, M.; Yu, X.H. A Robust Adaptive Terminal Sliding Mode Control for Rigid Robotic Manipulators. *J. Intell. Robot. Syst.* **1999**, *24*, 23–41.
37. Feng, Y.; Yu, X.H.; Man, Z.H. Non-Singular Terminal Sliding Mode Control of Rigid Manipulators. *Automatica* **2002**, *38*, 2159–2167. [CrossRef]
38. Mondal, S.; Mahanta, C. Adaptive Second Order Terminal Sliding Mode Controller for Robotic Manipulators. *J. Frankl. Inst. Eng. Appl. Math.* **2014**, *351*, 2356–2377. [CrossRef]
39. Cazzolato, B.S.; Prime, Z. On the Dynamics of the Furuta Pendulum. *J. Control Sci. Eng.* **2011**, *2011*, 8. [CrossRef]

Disclaimer/Publisher's Note: The statements, opinions and data contained in all publications are solely those of the individual author(s) and contributor(s) and not of MDPI and/or the editor(s). MDPI and/or the editor(s) disclaim responsibility for any injury to people or property resulting from any ideas, methods, instructions or products referred to in the content.